上海交通大學

SHANGHAI JIAO TONG UNIVERSITY

学士学位论文

BACHELOR'S THESIS

论文题目:移动情况下分子通信调制技术的研究

学生姓名: 常　歌

学生学号: 5130309108

专　　业: 测控技术与仪器

指导教师: 闫浩

学院(系): 仪器科学与工程系

Submitted in total fulfillment of the requirements for the degree of Bachelor in Measurement and Control Technology and Instruments

Adaptive Detection and ISI Mitigation For Mobile Molecular Communication

GE CHANG

Advisor
Assistant Prof. HAO YAN

DEPARTMENT OF INSTRUMENT SCIENCE AND ENGINEERING
SCHOOL OF ELECTRONIC INFORMATION AND ELECTRICAL ENGINEERING
SHANGHAI JIAO TONG UNIVERSITY
SHANGHAI, P.R.CHINA

June 17, 2017

移动情况下分子通信调制技术的研究

摘　要

新兴的纳米技术的发展使得纳米机器摆脱了传统应用的桎梏，具有了解决新问题的可能。受限于纳米机器本身的尺寸和结构，单个的纳米机器只能执行非常简单的操作。因此，使得纳米机器相互联系成为纳米网络是将纳米机器投入复杂应用的必要条件。纳米尺度上，传统的无线通讯网络难以应用到纳米机器，而普遍存在于自然界中的分子通信却有可能成为纳米网络的最优解决方案。分子通信技术中的信息传输均以分子的形式进行编码，传输与接受均由纳米机器进行。

当前分子通信的研究主要集中在静态发射与接收器之间的调制与解调技术。但接收或发射器移动状态下分子通信同样需要被关注，目前为止，这一领域的研究仍然非常有限。在移动情况下的分子通信之中，距离的不断变化使得信道响应函数的幅值会不断产生变化，基于固定阈值的解调方法因此失效。码间串扰问题会因为幅值的变化而更加不可预测，影响解调过程的可靠性。在我们的工作中，我们提出了一种可适应的码间串扰解调方法以及两种动态解调方案。在我们的系统中，码间串扰的抑制与距离估计被应用在每一位的解调前处理之中，基于幅值和峰值时间的两种解调方法之后被用于信号的解调。

除此之外，针对静态条件下的高速分子通信场景，我们提出了局部拟合的方案，通过信号局部导数的求解进行判定，仿真证明我们提出的方案在高速率的情况下，具有较高的可靠性。

关键词： 分子通信，码间串扰，移动接收器，自由扩散，动态解调

Adaptive Detection and ISI Mitigation For Mobile Molecular Communication

ABSTRACT

The emerging nanotechnology enables biological nano-machines to deal with problems beyond the reach of traditional applications' tendrils. Limited by its size and structure, a bio-nanomachine is only capable of performing simple tasks. However, a bio-nanomachine preserves much potential to exploit in interfacing with other bio-nanomachines. While traditional wireless communication has difficulties to be applied in this scale, molecular communication is one kind of ideal communication paradigm for nano-networks being energy efficient as well as reliable. The transmission and the rec reception of information in molecular communication are encoded in molecules between different nano-machines.

Current studies on modulation and demodulation schemes in molecular communication mainly focus on the scenarios with static transmitters and receivers. However, mobile molecular communication is needed in many envisioned applications, such as target tracking and drug delivery. Until now, investigations about mobile molecular communication are very limited. In this work, mobile molecular communication with a mobile bacterium-based receiver performing random walk is investigated. In mobile scenario, system impulse response changes due to the dynamic change of the distance between the transmitter and the receiver. A fixed threshold fails in signal detection in the mobile scenario. Inter-symbol interference (ISI) is another problem in molecular communication. The decoding process will be interfered by residual molecules from former symbols. Furthermore, the ISI effect becomes more complex due to the dynamic character of the signal which makes the estimation and mitigation of ISI even more difficult. In this work, an adaptive ISI mitigation method and two adaptive demodulation schemes are proposed for this mobile scenario. In the proposed scheme, adaptive ISI mitigation, estimation of dynamic distance and the corresponding system impulse response calculation are performed in each symbol interval. Based on the dynamic system impulse response in each interval, two adaptive demodulation schemes, concentration-based adaptive threshold detection (CATD) and peak-time-based adaptive detection (PAD), are used for decision.

Besides, we introduce a non-coherent detection method utilizing the local derivative of the channel response. By local fitting (LF) technique, reliable decoding information can be abstracted from incomplete channel response. Therefore, this method can be applied for high bit rate scenario where heavy effect form ISI and following symbols exist. A generalized bit rate definition is introduced for proper performance evaluation and Bit Error Rate (BER) is employed to evaluate the performance of our detection method. Simulations demonstrate that the ISI effect is significantly reduced, and the adaptive demodulation schemes are reliable and robust.

KEY WORDS: Molecular communication, inter-symbol interference, mobile receiver, diffusion channel, adaptive demodulation

Contents

List of Figures vi

List of Tables vii

Chapter 1 Introduction 1

1.1 Coverage Problems 3

1.2 Contribution of This Work 4

1.3 Organization 5

Chapter 2 Related Work 6

2.1 Signal Detectors 6

2.2 Parameters Estimation 7

Chapter 3 Mobile Molecular Communication Scenario 9

3.1 System Model 9

3.1.1 Movement of Mobile Receiver 9

3.1.2 Diffusive Communication Model 11

3.2 Problem Statement 14

Chapter 4 Proposed Schemes And Simulations For Mobile MC 17

4.1 Proposed Demodulation Scheme 17

4.1.1 Overall Scheme 17

4.1.2 Demodulation 18

4.1.3 Accuracy Analysis and Parameter Design 23

4.1.4 ISI mitigation 25

4.2 Simulation Results 30

4.2.1 Simulation Parameters 30

4.2.2 Investigation of Symbol Sequence Length 31

4.2.3 Investigation of Symbol Interval 34

4.2.4 Investigation of Initial Distance 35

4.2.5 Investigation of Sampling Number in An Interval 36
4.2.6 Investigation of Noise 37
4.2.7 Summary 38

Chapter 5 High Bit Rate Static MC Scenario 39

5.1 System Model 40
5.1.1 Channel Model 40
5.1.2 Bit Rate 41
5.2 Local Fitting Demodulation Scheme 41
5.2.1 MAP Coherent Detection in Previous Work 41
5.2.2 Local Fitting Demodulation 42
5.2.3 Noise Mitigation and Derivative Calculation 44
5.3 Simulation Results 44

Chapter 6 Conclusion 47

References 50

Published Papers during Undergraduate Study 57

Acknowledgements 58

List of Figures

1–1 ToC . . . 2

3–1 Mobile Receiver Trail . . . 10
3–2 Mobile IR Model . . . 12
3–3 IR Variation . . . 13
3–4 Adaptive Threshold in Static MC . . . 14
3–5 ISI Effect in Mobile MC . . . 16

4–1 Demodulation Scheme . . . 18
4–2 Samples in One Interval . . . 21
4–3 IR Reconstruction . . . 23
4–4 IR Reconstruction by Index . . . 25
4–5 IR with Different Distance . . . 27
4–6 ISI Mitigation Method . . . 28
4–7 Sequence Length . . . 33
4–8 Symbol Interval . . . 34
4–9 Initial Distance . . . 36
4–10 Sampling Number . . . 37
4–11 Impact of SNR . . . 38

5–1 Block diagram of the MCvD system . . . 40
5–2 Channel impulse response and its derivative. . . . 42
5–3 Local Fitting Detection . . . 45
5–4 Channel impulse response and its derivative . . . 46

List of Tables

4–1 Correlation Coefficients for Index Values 24
4–2 Simulation Parameters 30

Chapter 1 Introduction

Emerging nanotechnology promises the use of molecular communication (MC) in nanonetworks, by which biological nanomachines (bio-nanomachines) can communicate with each other by sending and receiving molecules[1]. Being highly efficient and low-cost[2], MC is prevalent in nature and human bodies, e.g., in cell-cell communication. With the help of nanotechnology, MC may facilitate a plethora of applications from nano-electromechanical systems (NEMS) to in-body health monitoring[3].

Nanomachine is the basic element in a MC system. Size of the nanomachine ranges from nanometers to micrometers. There are three different approaches for the development of nanomachines, including top-down approach, bottom up approach, and hybrid approach[1]. These approaches considering different communication layers as beginning. Genetically engineered cell is a good candidate for the development of bio-nanomachines. Among assorted cells that could be used as bio-nanomachines, flagellate bacteria are universally used in genetic engineering. For example, Escherichia coli (E. coli) is one kind of bacterium with flagella with the advantages of easy-producing, low-cost[4],[5]. It has been used as the communicating nanomachines in MC[6, 7].

MC for static nanomachines has been intensively studied in the past few years[8–12]. However, mobile MC is not paid too much attention to so far, although it can be envisioned as a potential scenario in many applications. There are a few researches on the mobile MC scenarios, a group of nanorobots could communicate and coordinate with each other to move towards cancer cells to release drugs[13]. In[14], digital MC systems in blood vessels were established, where the transmitter nanomachine is mobile. A clock synchronization scheme was proposed for a similar mobile scenario in[15]. In[16] and[17], fluorescence resonance energy transfer (FRET) based mobile molecular nanonetworks were considered. The communication theoretical analysis as well as coverage and throughput analysis were conducted. Another kind of mobile ad hoc nanonetworks is proposed for collision-based MC[13]. A positional-distance codes scheme was proposed for mobile MCs and a hardware experiment based on a macro-scale testbed was performed[18]. The mobility pattern of nanoparticles, e.g., E. coli, was described in[19]. A few investigations have been conducted on the demodulation schemes for mobile MC. In[20], the authors give a focus on the receptor process of the receiver for the derivation of the system’s

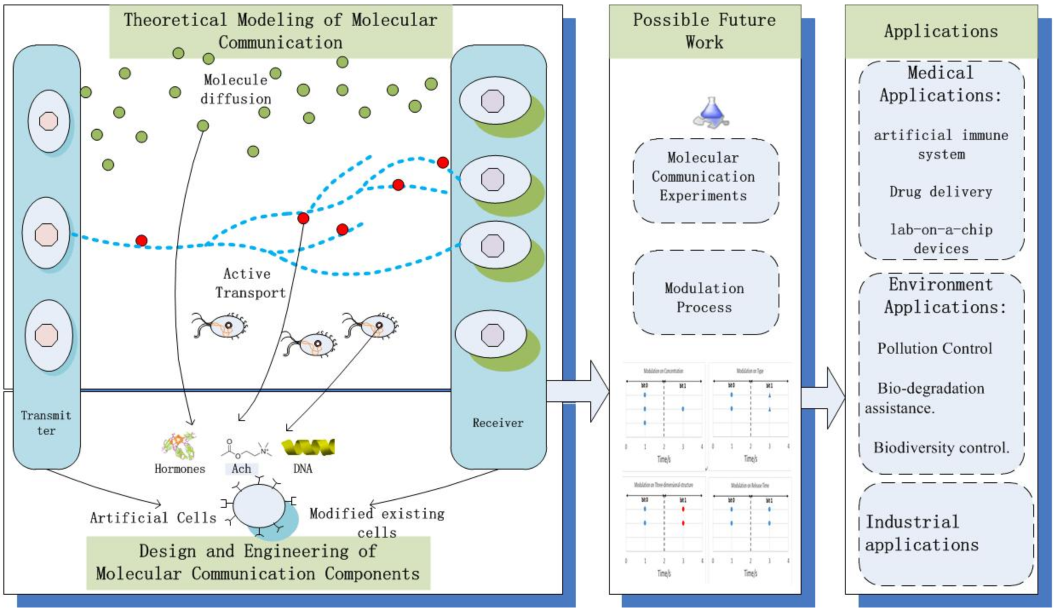

Figure 1–1 ToC of the MCvD system

CIR. However, a reliable detection scheme in mobile MC is still absent to the best of the authors' knowledge. Therefore, we try to pursue a better decoding performance in mobile MC in our work. Also, we try to find an ideal detector that can be applied both in static and mobile MC scenario.

In this environment, bio-nanomachine has a scope of nano-to-macro scale[3]. Nanoscale complexes include protein motors used to bind specific type of molecules[3] or DNA sequence, while genetically engineered cells are the represent of macroscale bio-nanomachines. According to the recent research in[2], genetically cells, which are under macro-scale, are still the most feasible ways to produce bio-nanomachines. As we can see from[2], basic approaches to produce bio-nanomachines with functionality are still on the scale of cells or cell-like structures. Therefore it would be relatively valuable to focus on the movement of the cell or cell-like structures, which has the potential to be used as the bio-nanomachine.

For example, Escherichia coli (E. coli) is one kind of bacterium with flagllum with the advantages of easy-producing, low-cost, etc.[4, 5]. In[7], E. coli is coordinated through the two types of signaling molecule as the bio-nanosensor. What's more, the motion characteristics of this kind of cells has been studied thoroughly, so we could predict its motion with more credibility[21].

However, so far, the modulation and the demodulation for mobile MC have not been investigated.

1.1 Coverage Problems

In this subsection, we focus on two problems: the feasible decoding scheme in the mobile MC scenario and the reliable detection in high bit rate.

In the mobile MC, two categories of problems arise. Both problems root in the random movement of the transmitter nanomachine and/or the receiver nanomachine. Assuming binary concentration shift keying (BCSK) modulation technique is used, a bit “1” is represented by sending Q molecules and a bit “0” is represented by sending nothing[22]. When the transmitter releases Q molecules, the molecules move randomly based on Brownian motion. According to the Fick’s second law of diffusion, the impulse response (IR) is a function of time and the distance between the transmitter and the receiver. The concentration at the receiver increases quickly until reaching its maximum, and decreases slowly, forming a long tail[23]. If the transmitter and the receiver are static, the IRs for bit “1” transmissions are always the same. However, if the transmitter and/or the receiver is mobile, then the IR varies due to the random change of the distance between the transmitter and the receiver. For example, if the transmitter and the receiver become closer,the peak amplitude of the IR increases while the peak time decreases. This fact will influence the correct detection at the receiver side if the demodulation scheme for the static transmitter/receiver is still used.

The random walk of the messenger molecules would limit the concentration of molecules, forming a long-tail IR with concentration and time at a fixed distance. Also, in the ideal situation, receiver is fixed or have a steady velocity. However, many kinds of receivers have their own motions characteristics judged by their scales and types[19]. Some nanoscale bio-nanomachines would obey the Brownian movements like messenger molecules (often referred to 1–100 nm), while macroscale bio-nanomahines such as genetically engineered cells would be propelled by themselves. E. coli is one type of bacterium with a group of flagellum. With the propel pf the flagellum, they would alternate their motions between ordered and out-of-ordered state, known as “Run” and “Tumble” mode together, E. coli could produce the motion resembling like random walk of the messenger molecules[19, 21].

Another problem is the inter-symbol interference, namely, ISI[24, 25]. ISI is caused by the long-tail of the system IR. The residual molecules in the long-tail from former symbols interfere with the current symbol. ISI is considered as the most important error source of detection. In the mobile MC with random walking nanomachine, ISI effect becomes more complicated because the number of residual molecules from former bits is changing also because of the movement of the nanomachine. In such case, the ISI effect is hard to calculate and to mitigate. Hence, current

ISI mitigation methods and adaptive threshold approaches for static MC such as[25] do not work anymore.

1.2 Contribution of This Work

In this paper, two parts of research are conducted and related research issues are stated separately.

In contrast to the studies on demodulation for the static MC, our work deals with the issues caused by the mobile feature. To the best of the authors' knowledge, ways to mitigate the effect of ISI for mobile nanomachine has never been studied. Current demodulation method for BCSK such as fixed or adaptive threshold cannot give a reliable judgment method on this situation. The main three contributions of this paper lie in the following three parts:

- A three-dimensional channel model is established considering the random motion of E. coli as the mobile receiver nanomachine.
- An adaptive ISI mitigation method is proposed for mobile MC.
- Two adaptive demodulation schemes are proposed for mobile MC.

Besides, we propose a low-complexity detector for molecular communication system in high bit rate. Displaying the channel impulse response of the MC via diffusion, we observe that the ascending part of the channel response (i.e. the interval before the concentration reaches its maximum value) is less interfered by ISI in the high bit rate transmission. By employing local fitting technique, we sample the information from the ascending and utilize it to judge the symbol value in the current interval. Pre-smoothing technique is also adopted to mitigate the effect the noise from the environment. As there is no need of information about the former symbol sequence, this method needs less computational ability and memory resources. Shown in the simulation resources, our proposed scheme is promising in decoding high bit rate signal in MC and robust to the noise and other channel parameters variations. The main two contributions of this paper lie in the following:

- A definition of generalized bit rate is given.
- A non-coherent detector for molecular communication system in high bit rate is proposed.

1.3 Organization

The remainder of this paper is organized as follows. In Chapter 2, the related work about demodulation studies for MC is discussed. In Chapter 3, mobility pattern of the receiver and the channel model is given. The ISI as well as the mobile environment problems are stated. Chapter 4 proposes the detection schemes for the mobile MC. In Chapter 5, the local fitting scheme is proposed for the high bit rate MC scenario, the system model and the generalized definition of bit rate are also given. Simulations are conducted in this section. Finally, Chapter 6 concludes this paper.

Chapter 2 Related Work

In this section, the related work on demodulation in MC is presented. Due to the channel property, the modulated signal waveform at the receiver side spreads. Demodulation refers to the process of extracting the original information from the received signal after the transformation through the channel. In addition, the channel noise, such as additive noise or ISI, corrupts the modulated signal, which makes the demodulation more difficult.

The research works about signal detection and receiver design are highly related to the demodulation, therefore they are also included in this section.

2.1 Signal Detectors

Different types of modulation techniques need different demodulators. For MC, concentration-based modulation and type-based modulation are the two main widely used modulation techniques[26, 27]. Many works focus on the demodulation issues for either concentration-based modulation[8, 9, 22, 24, 25, 28–31] or type-based modulation[32, 33], or concentration and type combined modulation scheme[34]. In this paper, we focus solely on the concentration-based modulation such as on-off keying (OOK).

The basic process for demodulation include two steps: 1 sampling the received signal and 2 comparing the sample with a threshold to make a decision. An important issue in the demodulation process is to remove ISI. Increasing time interval may be one solution to mitigate the effect of ISI. However, this sacrifices the data rate, which is undesirable. The existing research works proposed different demodulation schemes balancing the probability of error and computational complexity for different data rates. Some adaptive detection methods are proposed for better decoding performance considering the ISI effect. In[22], the authors proposed two demodulation schemes, namely, sampling-based detection and energy-based detection for OOK modulation techniques. The receiver samples the molecule concentration at a time or accumulates the molecule concentration for a bit period, hen the result is used for decision making. In[28] and[31], theoretical formulations and architectures of the strength-based optimum receivers based on spike transmission of molecules were presented in the presence of both diffusion noise and ISI. The optimum and suboptimum versions of ASK and OOK receivers were designed. In[9], the authors proposed sequence detection methods based on a posteriori (MAP) and maximum likelihood (ML) criterions. A linear equalizer based on minimum mean-square error (MMSE) criterion and a decision-feedback equalizer (DFE) were also proposed which reduced the probability of error detection. Similar ideas were proposed in[35], which accounts for the possibility of the presence of the steady uniform flow in any arbitrary direction, sources of information molecules in addition to the transmitter, and enzymes in the propagation environment to degrade the information molecules. In[25], an analytical technique is proposed to determine the optimum threshold. A new modulation namely molecular transition shift keying (MTSK) were proposed to decrease the effects of ISI and enhance energy efficiency. A power adjustment technique that utilizes the residual molecules were proposed. A low-complexity non- coherent signal detection for nanoscale MCs was proposed which can suppress ISI effectively[24]. In[36], a detection algorithm for a molecular multiple-input multiple-output scenario is proposed.

2.2 Parameters Estimation

Current ISI mitigation and demodulation methods are based on the situation where the distance between the transmitter and the receiver is fixed. Because the distance in the whole communication does not change, the IRs for the same symbols are the same. When the former symbol values are known, ISI effect on the current symbol is predictable. However, in the scenario of the mobile MC, the distance between the transmitter and receiver changes all the time due to the random movement of the nanomachines. The corresponding IR at the receiver changes accordingly. This means we cannot obtain a fixed optimal threshold for demodulation for all the transmitted symbols. Therefore, the proposed demodulation schemes in the literature without considering the mobility of the nanomachines will not work effectively anymore. Furthermore, the existing ISI mitigation method based on fixed IR is also not valid for the mobile scenario. Even if the former symbols are correctly predicted, the residual number of molecules at the receiver changes because the receiver moves randomly. Therefore it is almost impossible to correctly estimate or predict ISI. Therefore the existing demodulation proposals for static nanomachines are no longer applicable for the mobile scenario.

There exist a few works about parameter estimation in molecular communication, which may be helpful for distance estimation. In[37], two types of molecules are released in one interval. Based on the difference of their diffusion coefficient, the distance can be calculated from single spike feedback signal. In[38] and[39], a ML estimator for the distance was also proposed in an unbounded environment and the performance is close to the derived Cramer-Rao lower bound. In[40], two distance estimation schemes are proposed based on the peak concentration time and the concentration energy. In this paper, a demodulation scheme with ISI mitigation method suitable for mobile MC is proposed.

Chapter 3 Mobile Molecular Communication Scenario

3.1 System Model

The establishment of a system model must be compatible with application situation and hardware design. In our system design, a medium range (μm to mm)[41] MC between a fixed transmitter and a mobile receiver performing random walk in the human intestinal tract[42] is considered. The transmitter is modeled as a fixed point. One kind of flagellated bacterium, *E. coli* with radius a, is adopted as the mobile receiver[19].

In the first subsection, according to E. coli's characteristics, the receiver's mobility is modeled. In the second subsection, a mobile three-dimensional channel model of MC via diffusion is introduced by incorporating the receiver's mobility. Synchronization among nanomachines is assumed to be achieved[15]. The unit time in our model and simulation is set as Δt.

3.1.1 Movement of Mobile Receiver

As a well studied prokaryotic cell, E. coli is frequently used in biological engineering. It has a group of flagellum to decide its motion status, which falls into two categories, "Run" mode and "Tumble" mode[7].

In the "Run" mode, E. coli executes a linear motion with a steady velocity V_r. In the "Tumble" mode, E. coli deviates from its original direction with an angle $\pm\Delta\theta_{xy}$. Poisson distribution is adopted to describe the alternation between two modes[43]. For each unit time, the occurrence of the "run" mode has a constant probability λ and "tumble" mode's occurrence probability is 1-λ. The probability that run occurs between time t and $t + \Delta t$ is:

$$P(t; \lambda)\Delta t = \lambda e^{-\lambda t}\Delta t \tag{3–1}$$

For each tumble, the receiver would change its direction from θ to $\theta \pm \Delta\theta_{xy}$[7]. The mean-square angle deviation in time t is

$$\langle \theta^2 \rangle = 2D_r\Delta t, \tag{3–2}$$

where D_r is the rotational diffusion constant[19]. This can be obtained through Einstein-Smoluchowski relation in (3–3):

$$D_r = \frac{k_b T}{f_r}, \tag{3–3}$$

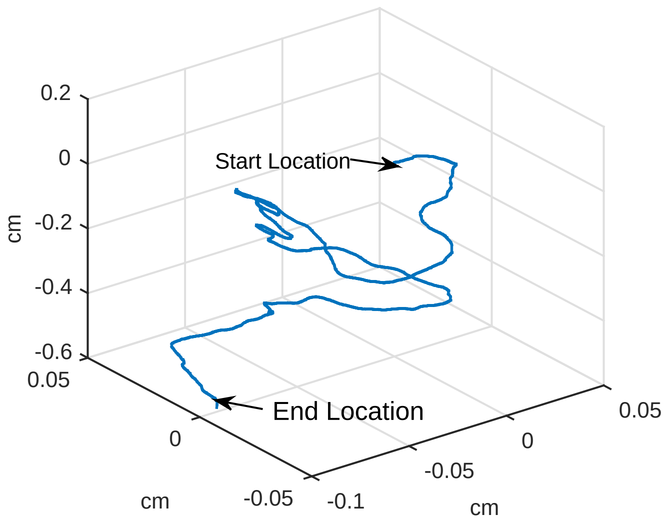

Figure 3–1 Mobile receiver's motion trail. Based on the E. coli's mobility pattern, the trail of the receiver is simulated with 500000 steps. The initial position of the receiver is $(0, 0, 0)$ and it has a initial velocity V_r along the x axis. Note that this is just an instance of the receiver's trail.

where k_b is the boltzman constant, T is the absolute temperature in the environment and f_r is the rotational frictional drag coefficient.

In three dimensional isotropic environment, that is, a two-dimensional rotational random walk, motions in different axis are statistically independent[19], therefore we have

$$\langle\theta^2\rangle = \theta_{xy}^2 + \theta_z^2 = 4D_r\Delta t, \tag{3–4}$$

where θ is the current angle and θ_z represents the angle of the receiver deviates from z axis. The location changes in each step are Δx, Δy, Δz distinctively.

$$\begin{aligned}\Delta x &= V_r\Delta t \sin\theta_z \cos\theta_{xy}\\ \Delta y &= V_r\Delta t \sin\theta_z \sin\theta_{xy}\\ \Delta z &= V_r\Delta t \cos\theta_z.\end{aligned} \tag{3–5}$$

If the receiver starts moving from (x_0, y_0, z_0), the current distance would be

$$d(t) = \sqrt{(x(t) - x_0)^2 + (y(t) - y_0)^2 + (z(t) - z_0)^2}. \tag{3–6}$$

With a motion uncertainty in each step, the receiver performs random walk in a three dimension environment shown in Fig. 3–1. Cartesian coordinate is used to describe the location of the receiver. Note that the rotational diffusion coefficient varies in different environments and will largely determine the motion trail of receiver such as E. coli[10].

As a small direction deviation leads to a totally different motion trail for a receiver, it is hard to predict future location with certainty in random motion.

3.1.2 Diffusive Communication Model

In an isotropic environment without fluid velocity, messenger molecules diffuse according to concentration gradient. The molecules' diffusion behavior is described by Fick's second law as[10]

$$\frac{\partial p(d,t|d_0)}{\partial t} = D\nabla^2 p(d,t|d_0), \tag{3–7}$$

where ∇^2, $p(d,t|d_0)$, d_0 and D are Laplacian operator, molecule distribution function, the initial distance between the receiver and the transmitter, and diffusion coefficient of the message molecule respectively.

Channel IR with a fixed distance d between the transmitter and the receiver is expressed as[19]

$$C(d,t) = \frac{V_R N}{(4\pi D t)^{\frac{3}{2}}} \exp\{-\frac{d^2}{4Dt}\}. \tag{3–8}$$

where the transmitter will send N molecules for symbol "1" each time. V_R represents the volume of the spherical receiver area. By substituting d in (3–8) by variable $d(t)$ in (3–6), the channel IR for a mobile receiver is

$$C(t) = \frac{V_R N}{(4\pi D t)^{\frac{3}{2}}} \exp\{-\frac{d^2(t)}{4Dt}\}. \tag{3–9}$$

In[12], there are two types of noise sources in molecular communication via diffusion: physical-sampling noise and physical-counting noise. Also, the external additive noise is considered and its impact on the receiver is derived in[44]. Since the physical sampling noise is negligible in the discrete binary concentration modulation[45] and we assume there is no other sources in the environment, we only include counting noise in our study. The counting noise is the counting error at receiver. It is generated due to the randomness of molecules in the movement and to the discreteness of the particles diffusion process and the limited sensing sensitivity of the receiver[12]. The counting noise $n_{cs}(t)$ is assumed to be independent and identically distributed (i.i.d) zero-mean white Gaussian noise[45][46]:

$$n_{cs}(t) \sim \mathcal{N}(0, \sigma_c^2(t)) \tag{3–10}$$

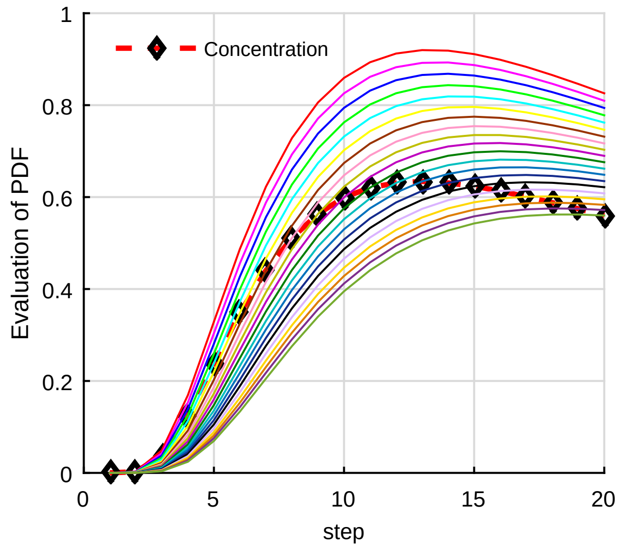

Figure 3–2 True IR in one interval with twenty steps. The receiver performs random walk and records signals with such twenty steps in an interval. Twenty different IR profiles determined by twenty different distances at these steps with (3–8) are shown in different colors. The corresponding values of these IRs at the twenty steps are highlighted by black diamond marks which forms the true IR in this interval. The plots other the bold red marked one are the IR plot based on the static distance in different time. Note that we have set the velocity larger than the actual situation to clarify the fluctuation in one interval. Also, this is an evaluation of a PDF under 1×10^5 molecules in one release.

As the Brownian motion is conducted independently by each molecule in the medium, the noise at different time is indpendent[45].

In our channel model, one interval is divided into multiply steps to include the distance change caused by the receiver's random walk in our simulation. Hence, each step has a new distance d_m $(m = 1, 2, \ldots, N_s)$ and a corresponding channel IR value C_m $(m = 1, 2, \ldots, N_s)$ within an interval according to (3–8). If we consider the channel IR in an interval, it is a composite of individual values C_i as shown in Fig. 3–2. The amplitude of this true IR in one interval fluctuates due to the randomness of distances. These multiply points are on the different IR plots based on different physical distance due to the random nature of the receiver. Therefore the true IR cannot be exactly expressed or fitted by one individual equation as in (3–8) with a constant d. However, a good estimate of the true IR by a reconstructed IR with a constant d is possible. This will be discussed in Section V.

Furthermore, from a macroscale perspective, true IRs are different even with the same transmitted symbol value due to the randomness of positions caused by random walk as illus-

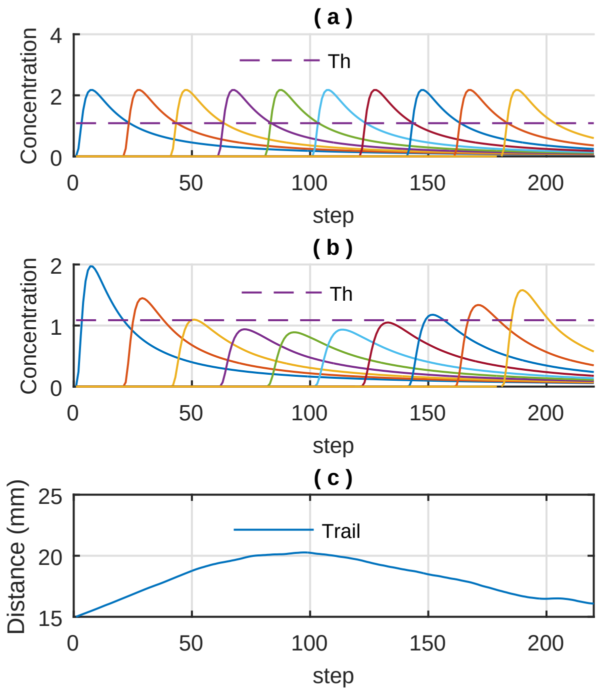

Figure 3–3 Channel IRs in static MC and in mobile MC. The transmitted symbols are [1 1 1 1 1 1 1 1 1 1]. (a) channel IRs at the receiver with fixed distance between transmitter and receiver. Fixed distance between the transmitter and the receiver is 15 mm. (b) channel IRs at the random walking receiver. (c) random distances between the transmitter and the random walking receiver in the case of (b). adaptive threshold in (a) and (b) is defined as half of the peak value of the IR of the initial distance for signal detection. It is shown that, with the adaptive threshold, symbols are correctly detected in static MC in (a) while they are not correctly detected in mobile MC in (b).

trated by Fig. 3–3. Fig. 3–3 (a) shows the IRs of a series of symbol "1" with a fixed distance between the transmitter and the receiver while Fig. 3–3 (b) shows the IRs with variable distances for the mobile receiver. Fig. 3–3 (c) presents the corresponding random distance values in (b). When the distance is fixed, the IRs are the same for each symbol "1" as in (a). However, when the distance is randomly changing as in (c), the shapes of the IRs differ from each other for the same symbol value and the change of IRs is unpredictable due to randomness as in (b).

The receiver in our system is "passive" type. When a molecule enters into a receiver, it triggers the receiver and continues its brownian motion and can trigger the same receiver or other receivers in the future.

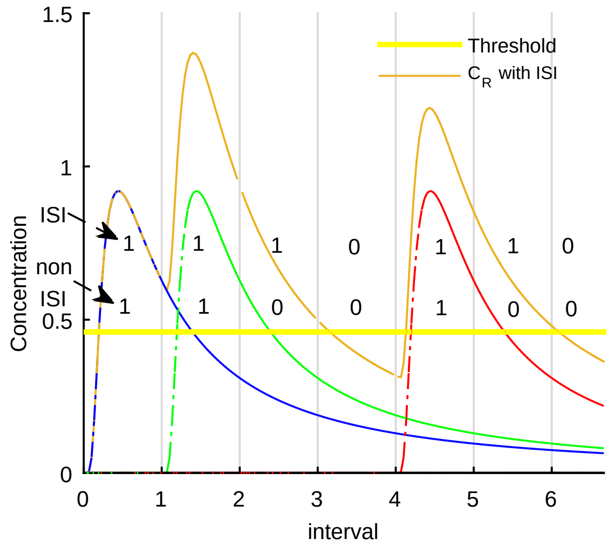

Figure 3–4 adaptive threshold demodulation for BCSK in non-mobile MC. The distance between the transmitter and the receiver is fixed during the communication and each symbol interval consists of 30 steps. Diffusion coefficient is 5 rad^2/s and symbol sequence from the transmitter is [1 1 0 0 1 0 0]. The adaptive threshold is set as half of the peak concentration value. Leaving aside ISI, the demodulated signal would be [1 1 0 0 1 0 0], however, with ISI effect, the demodulated result would be [1 1 1 0 1 1 0].

3.2 Problem Statement

Due to the mobility of the receiver, the IR is random. Such randomness complicates the ISI effect. The combination of the randomness of IR and complicated ISI further degrades the received signal in mobile MC.

Firstly, mobility may cause false detection. As discussed in Fig. 3–3 (b), a predetermined threshold fails in signal detection due to the randomness of the IR amplitude caused by the randomness of the distance and Brownian motion of the information molecules. Especially in the situation that the distance increases shown in the first half in Fig. 3–3 (c), the amplitude of IR decreases. If the amplitude decreases to the value smaller than the threshold, symbol “1” is misdetected as “0”.

Secondly, ISI effect distorts the received signal. In the mobile scenario, this situation becomes more complicated:

1 In an isotropic environment, it is unavoidable that some messenger molecules would arrive at the receiver after their symbol interval and therefore interfere with future symbol molecules, which causes ISI[25]. In the case of a fixed distance, the ISI effect of a former sym-

bol in a following interval is determined by the time lag between the intended interval of the former symbol and the following interval. Except from the first symbol interval, the molecules detected by the receiver are the accumulation of messenger molecules from intended symbol and residual molecules from former symbols[24]. For the ith symbol, the concentration detected by the receiver is

$$C_R^i(t) = C_i(t) + \sum_{k=1}^{i-1} C_k(t - kT_b) + n_{cs}(t) = C_i(t) + C_{\mathrm{ISI}}(t) + n_{cs}(t), \tag{3–11}$$

where $C_R^i(t)$ is the overall received concentration, $C_i(t)$ is the concentration of the intended symbol, and C_{ISI} is the concentration of ISI which is the sum of the concentrations of all the residual molecules from former symbols. The receiver cannot distinguish the concentration of intended molecules $C_i(t)$ from received concentration $C_R^i(t)$. Therefore, ISI further causes incorrect signal detection. This phenomenon with a fixed distance is illustrated in Fig. 3–4. The symbol sequence sent by the transmitter is 1100100. The dash-dot curves are the IRs for each symbol. The solid plot is the received concentration $C_R(t)$ including the ISI effect. The 3th and 6th symbols are incorrectly detected as “1” due to the ISI effect.

2 In mobile MC, mobility complicates the ISI effect. On one hand, ISI is determined by the concentration spread (long tail) of previous symbols as in the fixed distance scenario. On the other hand, the changing distance between the transmitter and the receiver makes the IR changing and further the long tail varies. Fig. 3–5 illustrates the ISI effect in a mobile MC. Only one symbol “1” is transmitted by sending N molecules. Its ISI effects at the receiver on the following three intervals are considered. The distance of the total four intervals are 27, 30, 33 and 23 mm respectively. To clarify the ISI change due to the distance change, the distance value is set as a constant value. The channel IRs in different intervals are different depending on their random distances. The dashed green, the dotted pink, the solid yellow and the dash-dot red curves are the IRs in the 1st (27 mm), 2nd (30 mm), 3rd (33 mm) and 4th (23 mm) intervals. Take the ISI in the 2nd interval (30 mm) for example. Its random IR is the dotted pink curve. The ISI effect of the transmitted symbol on the 2nd interval is black circles on the dotted-pink curve. Similarly, the ISI effect of the transmitted symbol “1” in the 3rd and 4th interval are the highlighted black circles on the solid yellow and dash-dotted red curves, respectively. Therefore, we can see that the ISI in mobile MC is affected by a varying IR. We should note that Fig. 3–5 only illustrates the ISI from one transmitted symbol “1”. However, ISI is the accumulated interference from all former symbols. This makes the signal degradation more complicated. Hence investigation of demodulation schemes suitable for the mobile MC is quite necessary.

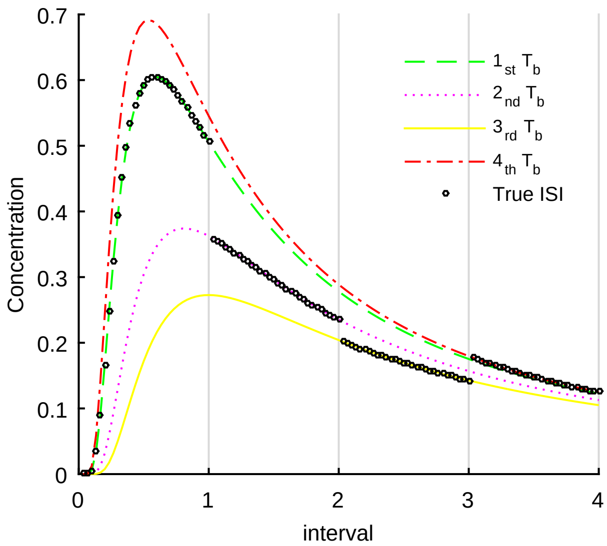

Figure 3–5 The transmitter sends a symbol "1". The ISI effect of this single symbol on the following intervals are considered in this example. The dashed green, dotted pink, solid yellow, and dash-dotted red curves are the IRs at the receiver with different distances in the 1st, 2nd, 3rd, and 4th interval which are 27 mm, 30 mm, 33 mm, 23 mm, respectively. The black circles on the green, pink, yellow, and red curves are the real concentrations at the mobile receiver for the four intervals. The ISI effects for 2nd, 3rd, and 4th intervals are highlighted by the black circles on the pink, yellow, and red curves.

Chapter 4 Proposed Schemes And Simulations For Mobile MC

4.1 Proposed Demodulation Scheme

In this section, we propose a demodulation scheme for the mobile MC with a mobile receiver. The proposed scheme includes an adaptive ISI mitigation method, distance estimation and IR reconstruction, and two adaptive signal detection methods. The aim of the proposed scheme is to solve the problem caused by mobility and complicated ISI in the mobile MC and to provide a solution for correct demodulation for the mobile MC.

4.1.1 Overall Scheme

Our proposed signal demodulation scheme for the mobile MC is illustrated in Fig. 4–1. Firstly, samples are taken by the receiver. Next the receiver judges whether the samples are the first symbol. A simple method could be like this: the receiver senses the environment. Once the environmental concentration is higher than a threshold after a long time silence, it is considered as the first symbol. If the symbol is the first symbol, we use the samples to estimate the current distance. Based on the estimated distance, the IR for the current interval is reconstructed. The next step is adaptive signal detection. Two adaptive detection methods, concentration-based adaptive threshold detection (CATD) and peak-time-based adaptive detection (PAD) methods, are proposed by comparing the sample values with the reconstructed IR. The detection result and the estimated distance are stored for the ISI calculation in the following interval.

If the symbol is not the first symbol, ISI mitigation is performed before distance estimation, IR reconstruction and adaptive signal detection. The ISI reduced data are used in the procedures including distance estimation, IR reconstruction and adaptive signal detection. The reason that the ISI mitigation is implemented before the distance estimation and IR reconstruction is to reduce the influence of the ISI effect and therefore to guarantee the accuracy of the distance estimation and the IR reconstruction and signal detection in the following steps.

The functional blocks including adaptive ISI mitigation, distance estimation and IR reconstruction, and CATD/PAD detection, are discussed in the following subsections in detail.

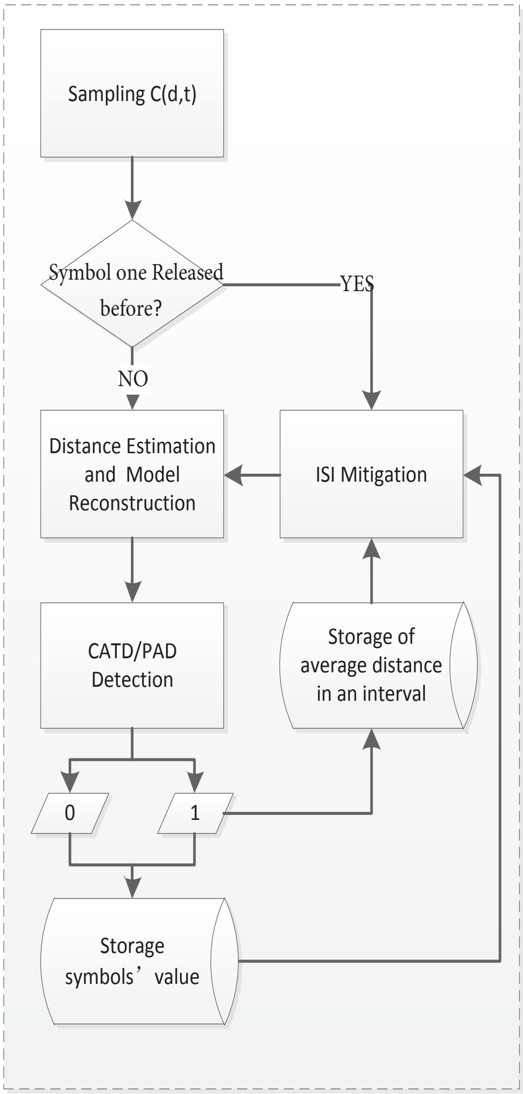

Figure 4–1 Demodulation scheme in one interval.

4.1.2 Demodulation

For the symbols without symbol "1" in the previous sequence, after sampling, the distance estimation and the IR reconstruction are performed. If the symbol "1" is included in the ISI sequence, the distance estimation and the IR reconstruction are performed on the ISI reduced data after ISI mitigation. In this subsection, when we talk about samples and data, we mean the samples without ISI in the first interval or ISI reduced samples from the second interval by default.

In the static MC with a fixed distance, decisions are made by directly comparing sample values with a threshold which is derived from the amplitude of the IR. However, this does not work for the mobile MC with random distance. In a mobile MC, the distance changes randomly. The IR which is a function of distance d as in (3–8) also changes randomly. In order to make correct decision, the threshold should also be changed accordingly in different intervals. In such case, a fixed threshold does not work in the mobile MC.

The key difference of the mobile MC from the static MC is the dynamic distance. If the random distance is known, all the problems discussed above could be solved. Herein we propose a demodulation scheme to solve this issue. The demodulation process is as follows. We use samples to estimate the dynamic distance and reconstruct the IR for the current interval. Then we compare the samples with the reconstructed IR to make decision for signal detection.

4.1.2.1 Distance Estimation and IR Reconstruction

The first step in the proposed demodulation scheme is to estimate the dynamic distance with the samples and use the dynamic distance to reconstruct the according dynamic IR in one interval. Previous works have proposed some methods on the parameter estimation especially on the distance estimation. In[37], two types of molecules are released in one interval. Based on the difference of their diffusion coefficient, the distance can be calculated from single spike feedback signal. In[38], for an unbounded environment, The Cramer-Rao lower bound on the variance of the distance estimation error is derived. A ML distance estimator is also proposed and the performance is close to the Cramer-Rao lower bound. In[40], two distance estimation schemes are proposed based on the peak concentration time and the concentration energy.

In our mobile MC, the mobile receiver performs multiple steps of random walk in an interval,say twenty steps. Due to the limitation of the energy supply of nanomachines, sampling at each step is energy consuming and not necessary. Our strategy is to take limited samples uniformly in one interval. Other sampling strategies are also possible. The influence of different sampling strategies on the estimation accuracy is little and can be ignored. With our sampling strategy, the samples (t_m, C_m) with $m = 1, 2, .., N_s$ as in (4–1), are uniformly taken within one interval as shown in Fig. 4–2. With an sample interval T_s, the m_{th} sample's time in i_{th} interval can be expressed as $t_m^i = t_1^i + (m-1)T_s$. With (t_m, C_m) $(m = 1, 2, .., N_s)$,.

$$C_R^i(t_m^i) = C_i(t_m^i)S_t^i + \sum_{k=1}^{i-1} C(t_m^i - iT_b)S_k^t + n_{cs}(t) \tag{4–1}$$

S_t^i is the i_{th} symbol value from the transmitter side.

After the ISI mitigation stated in the following subsection, we can obtain the ISI mitigated signal C_{RAM} and we utilize this signal to calculate the distance. d_i is solved by (4–2).

$$d_m = |2(-Dt_m^i \ln \frac{C_R^i(t_m^i)(4\pi Dt_m^i)^{\frac{3}{2}}}{N})^{\frac{1}{2}}| \qquad m = 1, 2, \ldots, N_s, \tag{4–2}$$

The average distance d_{ave} calculated in (4–3) is the estimated distance for this interval. The averaging is to mitigate the impact of the counting noise in the estimation.

$$d_{\text{ave}}^i = \frac{\sum_{m=1}^{N_s} d_m}{N_s}, \tag{4–3}$$

Also, it aims to obtain a distance which can better resemble the true CIR. In each interval, the receiver's random walk has a range. The physical meaning of d_{ave} is the estimation of the average position of the receiver in this interval. Due to the randomness, different intervals have different values of d_{ave}. Accordingly, the IR in each interval could be estimated by (4–4) with d_{ave}. If d_{ave} is a good estimation of the distance range in an interval, C_{ave} in (4–4) could be a good estimation of the true IR in the interval.

$$C_{\text{ave}}(t) = \frac{N}{(4\pi Dt)^{\frac{3}{2}}} \exp(-\frac{d_{\text{ave}}^2}{4Dt}). \tag{4–4}$$

4.1.2.2 Adaptive Signal Detection

In this work, two adaptive detection methods for the mobile MC are proposed.

The commonly used signal detection method in the static MC fails in the mobile MC. In the static MC, signal detection is usually performed by comparing the amplitude of samples in one interval with a fixed threshold. In the mobile MC, it is impossible to distinguish the symbol "1" or "0" purely from the received samples's amplitude. In an ideal situation without ISI in BCSK modulation, IR will be a long-tail curve for symbol "1" while no molecules are received for symbol "0". However, in practice, this is not the case. There are molecules received for symbol "0" even after ISI mitigation. This is because ISI mitigation method cannot remove ISI completely. Mobility further worsens such situation. In the mobile MC, ISI is more complicated and the mitigation is even harder to be complete. Besides ISI, other noise sources also exist such as the counting noise at the receiver side. Therefore, the received samples' amplitude are not zero for symbol "0" in practice. In the mobile MC, the amplitude of IR for symbol "1" is random

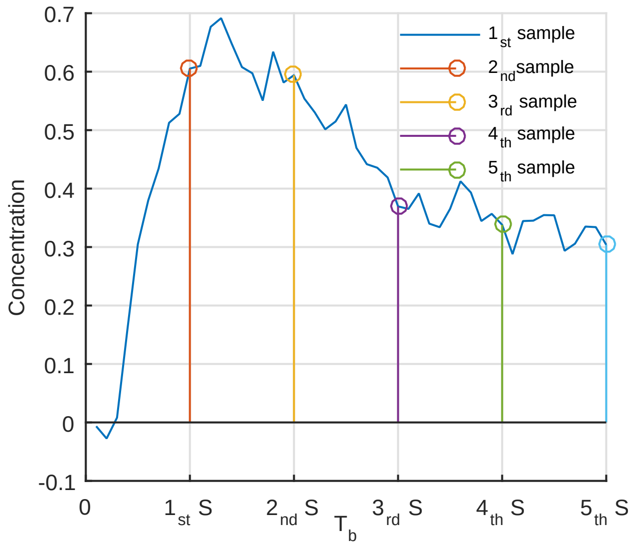

Figure 4–2 Samples in one interval. During one interval, five concentration samples are taken.The blue curve is the concentration curve and the five points on it are the samples taken. Samples are used to estimate the distance d_{ave} in this interval by (4–2) and (4–3) and then to reconstruct the IR in this interval by (4–4). These samples are included in one symbol interval TB. 1_{st} S here is the abbreviation of the first sample.

due to the receiver's random walk. It is difficult to distinguish the received samples are from symbol "1" or "0" purely from the amplitude in such complicated situation of MC. Therefore adaptive signal detection methods are needed herein.

In our proposed method, we use samples to estimate the distance and reconstruct the IR regardless of symbol value "0" or "1". However, for symbol "0", both the estimated distance and reconstructed IR are incorrect. This is because the samples used are residual ISI and the noise where no information is included. Luckily, there are characteristics in the IR to help judge the correctness of the IR reconstruction. By judging the correctness of the IR reconstruction, symbol values are judged. If the reconstructed IR is correct, the symbol is detected as "1" and otherwise "0".

Fig. 4–3 illustrates such characteristics. Two situations with symbol value "0" and "1" are shown respectively. In the case that the transmitted symbol is "0" (left pane), the received signal in an interval is the blue curve which is composed by residual ISI and noises. Five samples pointed by the arrows are taken in one interval. Distance estimation and IR reconstruction are performed based on the samples. The reconstructed IR is the dotted red curve 1st M. In the case that the transmitted symbol is "1" (right pane), the received signal in one interval is the blue curve. Same processing procedures as for symbol "0" are performed. The reconstructed IR is the red dot-dashed curve 2nd M. By comparing the two reconstructed IRs in the two panes, it is seen that the reconstructed IR for symbol "1" fits the true signal well while the reconstructed IR for symbol "0" does not fit the true signal. In the case of symbol "0", the concrete differences of the reconstructed IR from received signal are in the characteristics of the amplitude and phase (peak time). The amplitudes of the samples are much smaller than the peak amplitude of the reconstructed IR. The peak time of the reconstructed IR falls outside of the current symbol interval. This is against common sense that, the peak point of IR should be within the symbol interval. Otherwise the main part of signal energy of a symbol will appear in the next interval and causes an unwanted interference.

Based on the above two characteristics in amplitude and phase respectively, we propose two adaptive detection schemes which are concentration-based adaptive detection (CATD) scheme and peak-time-based adaptive detection (PAD) scheme.

In CATD scheme, the sample amplitudes are compared with the reconstructed IR. A threshold $C_{\text{threshold}}$ and the decision rule is mathematically defined as (4–5) based on the peak value of the established IR.

$$B_n = \begin{cases} 1, & C_n \geq C_{\text{threshold}} = \alpha \times C_{\text{max}}, \\ 0, & \text{Otherwise} \end{cases} \tag{4–5}$$

where C_n is the maximum amplitude of the samples in the current interval and C_{max} is the peak amplitude of the reconstructed IR. If C_n is higher than $C_{\text{threshold}}$, the symbol is detected as "1", otherwise "0". The parameter α is determined by system parameters such as the noise and ISI effect. Investigated by Monte Carlo simulations, $C_{\text{threshold}}$ is set as 70 % of peak value when SNR is 22 dB and symbol interval is two times of the peak value time.The value of the metric might be set through the simulation. However, it may be adjusted according to the change of the system parameters. Furthermore, design of the threshold should be based on the analytical expression of the system error probability considering the noise and ISI effect.

In PAD scheme, decision is made by comparing peak time t_{peak} of the reconstructed IR and the symbol interval length. The time interval of the MC system is set larger than t_{peak} in the system design. In a reconstructed IR, t_{peak} is calculated by setting the derivative of (3–9) to zero and we obtain

$$t_{\text{peak}} = \frac{d_{\text{ave}}^2}{6D}. \tag{4–6}$$

The decision rule of PAD scheme is mathematically expressed as

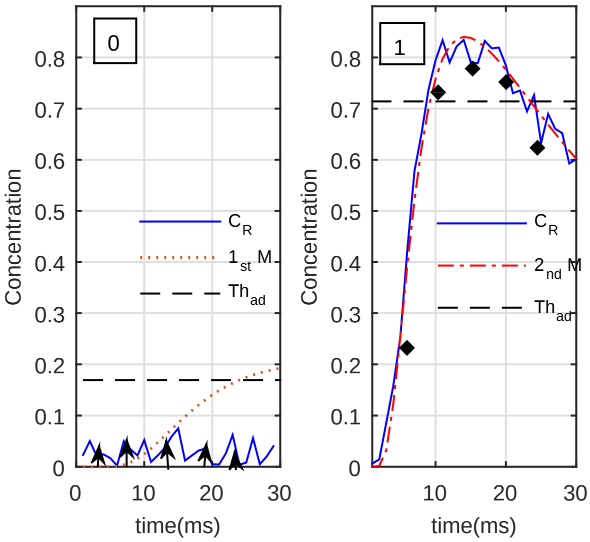

Figure 4–3 IR reconstructions for symbol “0”(left figure) and “1” (right figure). Blue curves are the received signal for symbol “0” and “1”. Red dotted and red dash-dotted curves are the according reconstructed IRs for symbol “0” and “1”, respectively. Arrows and diamonds are concentration samples.

$$B_n = \begin{cases} 1, & T_b \geq t_{\text{peak}}, \\ 0, & T_b < t_{\text{peak}}. \end{cases} \tag{4–7}$$

If the t_{peak} is larger than the current interval, the intended symbol is detected as “0”, otherwise “1”.

4.1.3 Accuracy Analysis and Parameter Design

The accuracy of both the ISI mitigation and proposed demodulation scheme rely on the accuracy of the distance estimation of d_{ave} in (4–3) and the corresponding reconstructed $C_{\text{ave}}(t)$ in (4–4). As discussed in Section IV, the reconstructed $C_{\text{ave}}(t)$ with a fixed distance d_{ave} cannot be exactly the same as the true IR in Fig. 3–2 which is a composite curve of the points from different IRs at different distances in one interval. However, a reconstructed $C_{\text{ave}}(t)$ can be a good estimation of the true IR. To quantitatively evaluate the estimation accuracy of $C_{\text{ave}}(t)$, correlation coefficient ρ is used to quantify the similarity of the reconstructed IR $C_{\text{ave}}(t)$ and true IR $C_{\text{true}}(t)$.

$$\rho = \frac{\text{Cov}(C_{\text{ave}}, C_{\text{true}})}{\sqrt{Var(C_{\text{ave}})}\sqrt{Var(C_{\text{true}})}}, \tag{4–8}$$

Table 4–1 Correlation Coefficients for Index Values

k	0.3%	3%	30%	50%
Correlation Coefficient	1	0.9985	0.8687	0.5631

where Cov(X, Y) is the covariance function of two variables X and Y, Var is the data's variance. Larger ρ indicates a larger similarity and therefore a better estimate. To achieve a good estimate of IR $C_{\text{ave}}(t)$, the average distance d_{ave} used to reconstruct IR should be a good estimation of the range of random walk in one interval. For this purpose, the range of relative distance change in one interval should be controlled in the previous system design. Herein we define relative distance change index k in (4–9) to calculate the maximum relative distance change in one interval.

$$k = \frac{d_{\text{max}}}{d_0} = \frac{V_r \times T_b}{d_0}, \tag{4–9}$$

where T_b is the time length of an interval and d_0 is the initial distance. d_{max} is the maximum possible distance change a receiver could reach in an interval. A larger k indicates the possibility of larger deviation in the estimated distance d_{ave} from the specific distances in one interval.

In order to study the impact of the relative distance change on the estimation quality of IR, the relation between the relative distance change index k and the correlation coefficient ρ is investigated by simulation. At different k values, the average distance d_{ave} is calculated and the according IR $C_{\text{ave}}(t)$ is reconstructed by (4–3) and (4–4). The result is shown in Fig. 4–4. The solid curves are the true IRs while the non-solid curves are the reconstructed IRs. The curves of same color are of the same set of data and k. As seen in Fig. 4–4, the true IR and the reconstructed IR fit well with each other with $k = 0.3\%$ and $k = 3\%$. However their difference gets larger when k increases. To quantify the similarity of true and the reconstructed IRs, correlation coefficient ρ in (4–8) is calculated and presented in Table 4–1 which shows that, coefficient ρ decreases when k increases. This quantitative result in Table 4–1 agrees with the result shown in Fig. 4–4 that similarity of the reconstructed IR and the true IR decreases when the relative distance range in an interval increases. With k less than 3%, the correlation coefficient ρ between our estimated IR and true IR is larger than 0.9985 which indicates that the established IR is a good estimation of the true IR. In this work, we define the situation with $k \leq 5\%$ as good conditions for estimation according to our investigation data.

Therefore, in order to achieve accurate IR reconstruction, system parameters including initial distance d_0, receiver velocity V_r, and interval length T_b should be designed to make the

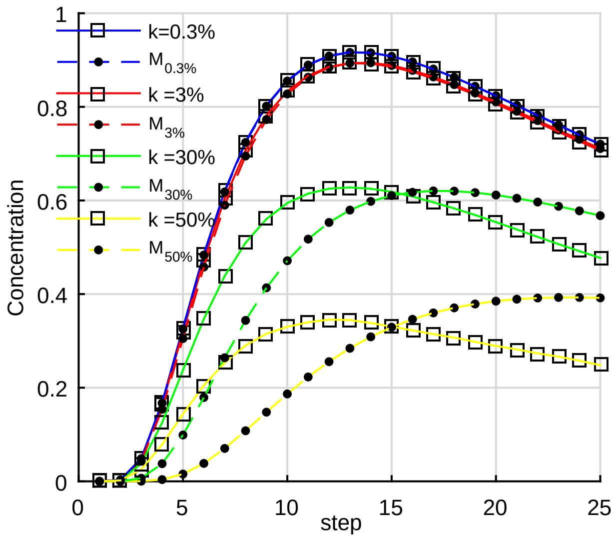

Figure 4–4 IR reconstruction with different values of k. Value of k changes from 0.3%, 3%, 30% and 50%. The solid blue, red, green and yellow curves are the true IR. The according reconstructed IRs with our proposed methods are presented by dashed blue, dotted red, dash-dotted green and yellow with circle dots respectively. The difference between true and reconstructed IRs gets larger with larger k.

index k be less than 5%. By controlling index k in this range, the reconstructed IR is a good estimation of the true IR. This accurate reconstructed IR is utilized in the signal detection and the ISI mitigation in the following intervals. Only with accurate IR, the accuracy of signal detection and ISI mitigation can be guaranteed.

4.1.4 ISI mitigation

ISI is an interference of former symbols to the current symbol. In our demodulation scheme, if the symbol is the first symbol, there is no ISI and we do not implement ISI mitigation. If symbol is not the first symbol, ISI exists and ISI mitigation is implemented before other steps to eliminate its impact on the following steps in current interval and to improve the accuracy of the whole demodulation scheme.

To implement ISI mitigation, the key issue is the calculation of ISI in current interval. To calculate ISI in the current interval, the values of former symbols and system IR in current interval should be known. However, IR randomly changes and is difficult to know in the mobile MC. This is because the position of the receiver in the mobile MC changes with its random walk. Only when the random distance between the transmitter and receiver is known, the IR in the current interval can be calculated. But, in our scheme, ISI mitigation is performed before the distance estimation in each interval. Therefore, the distance in the current interval and the corresponding IR is unknown when the ISI calculation is implemented.

To solve this key problem, we utilize the distance of last symbol "1" to approximate the distance in the current interval in ISI calculation. This distance can be expressed as d_{ave}^{i-l} and symbol sequence $[S_{i-l+1}, \ldots, S_{i-1}]$ are all symbol zero. The corresponding IR for mitigation is acquired by 4–10.

$$C_{\text{Re}}^{i}(t_m^i) = \sum_{k=1}^{i-1} C(d_{ave}^{i} - l, t_m^i - iT_b) S_k^d \tag{4–10}$$

For the ith symbol, the mitigated signal in i_{th} symbol is calculated by 4–11.

$$C_{RAM}^{i} = C_{R}^{i}(t_m^i) - C_{\text{Re}}^{i}(t_m^i) \tag{4–11}$$

However,the counting noise still exists during the distance estimation. Also, there are still some residual molecules after the ISI mitigation. Therefore, there is a difference between the true averaged distance and the approximate distance d_{ave}^{i}. This concentration error can be expressed in 4–12.

$$C_{e}^{i} = \sum_{k=1}^{i-1} C_k(t_m^i - kT_b) S_k^t + n_{cs}(t) - \sum_{k=1}^{i-1} C(d_{ave}^{i} - l, t_m^i - iT_b) S_k^d \tag{4–12}$$

A question arises that whether the approximation accuracy can be guaranteed. To answer this question, we firstly investigate the characteristic of the IR. As shown in Fig. 4–5 where IRs of the true averaged distance $d_{\text{ave}}(i) = 20$ mm and approximate distance $d_{\text{ApprDist}}(i) = 22$ mm are presented, the maximum amplitude difference is at the peak value. In MC, symbol interval T_b is usually set after the peak time to avoid severe symbol interference as in (4–13). Some detection methods have been proposed where the peak time can exceed the interval[45]. The long-tail part after the peak is where the ISI is calculated. In the long-tail part, it is seen that the amplitude difference of the two curves decreases rapidly with respect to time. Hence, it is possible to approximate one curve by another in the long-tail part far from the peak time as long as the difference of the two distances are not large. Therefore, that T_b is larger than the peak time and that the difference between the true average distance and the approximate distance is not too large are the two preconditions for the approximation. Based on the first precondition, we have (4–13). For the second precondition, let us recheck the relative distance change index k in (4–9) in the last subsection where we require $k < 5\%$ for accurate distance estimation in an interval. The physical meaning of this requirement is that the maximum distance change in an interval is less than 5% of d_0. This also guarantees that the distance change in nearby intervals is limited.

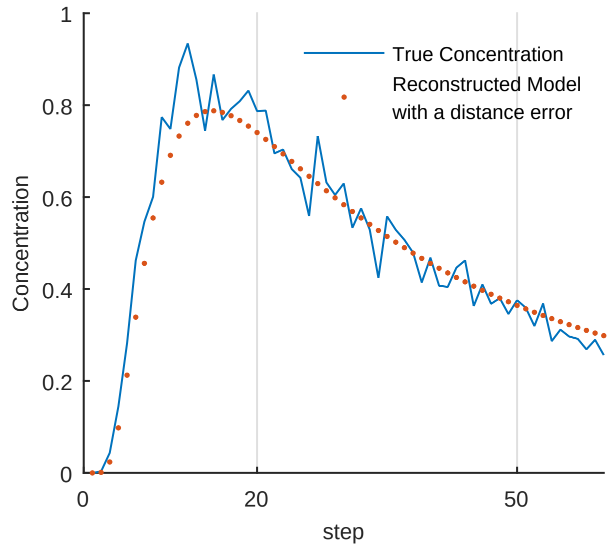

Figure 4–5 IRs of two different distances 20 mm (red) and 22 mm (black).

With constant velocity of the receiver V_r and the initial distance d_0, requirement $k < 5\%$ is rewritten as (4–14). Combining (4–13) and (4–14), we have (4–15) which expresses the two preconditions in our system. Next we check the accuracy of the distance approximation under the condition of (4–15). With different values of T_b in range of (4–15), IR reconstructed by the approximate distance $d_{\text{ApprDist}}(i)$ is compared with the IR reconstructed with $d_{\text{ave}}(i)$ in the current interval. Accuracy is quantitatively evaluated by correlation coefficient ρ of the two IRs. The result shows that the correlation coefficient ρ of the two IRs is better than 99.9987% under the condition of (4–15). This demonstrates that the approximate distance $d_{\text{ApprDist}}(i)$ is quite an accurate approximation of the current distance $d_{\text{ave}}(i)$ and the proposed ISI mitigation based on the approximate distance is feasible under the condition of (4–15).

$$T_b > T_{\text{peak}}, \tag{4–13}$$

$$T_b < 0.05\frac{d_0}{V_r}, \tag{4–14}$$

$$T_{\text{peak}} < T_b < 0.05\frac{d_0}{V_r}. \tag{4–15}$$

Next, the proposed adaptive ISI mitigation method and the demodulation scheme is illustrated by Fig. 4–6 by an example. The transmitted symbol sequence is [1 1 0] with BCSK

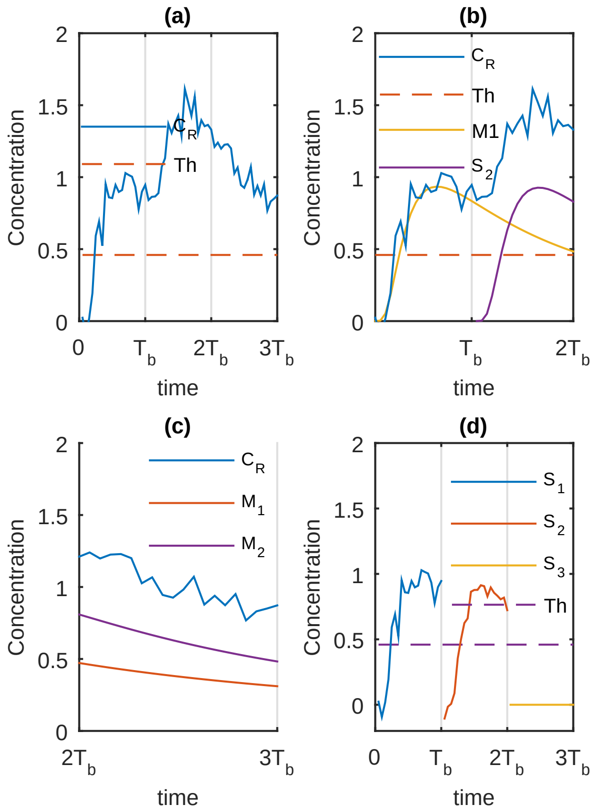

Figure 4–6 Illustration of the proposed ISI mitigation method. The plot M_{ab} in the figure is defined as the reconstructed model of symbol a in the b_{th} interval. Transmitted symbol sequence [1 1 0] is detected by the mobile receiver with BCSK modulation. (a) C_R is the concentration at the receiver and Th is the fixed threshold derived from the initial distance d_0 which fails in demodulation in mobile MC; (b) ISI mitigation in the 2nd interval; (c) ISI mitigation in the 3rd interval; (d) ISI mitigated signal by our proposed ISI mitigation method and symbols are demodulated properly.

modulation. With ISI, the true signal $C_R(t)$ at the receiver is shown in Fig. 4–6 (a). With a fixed pre-determined threshold Th defined as half of the peak amplitude of IR at initial distance d_0, the 3rd symbol is incorrectly decoded as “1”. The proposed adaptive ISI mitigation method and demodulation scheme is applied as follows. The receiver takes only limited samples of $C_R(t)$. In Fig. 4–6 (b), samples in the first interval are not affected by ISI. Therefore no ISI mitigation is implemented. The samples are directly used to estimate the distance and reconstruct the IR M_{11} with estimated distance shown by yellow curve in (b). By comparing reconstructed IR M_{11} and the samples of C_R taken in the 1st interval, adaptive signal detection method detects the symbol as "1". In the 2nd interval, ISI from the 1st symbol is firstly calculated and mitigated. At this moment, the distance in the 2nd interval is unknown. Because the last symbol is "1", the distance for the first symbol is used as the approximated distance and the IR M_{11} is used as the approximate IR in the 2nd interval for ISI calculation. With the demodulated value in the 1st interval and the approximate IR in the 2nd interval, the ISI in the 2nd interval is calculated by (4–11). By subtracting it from the received $C_R(t)$ (blue curve) in the second interval, the ISI mitigated samples on the purple curve S_2 is obtained in (b). Note that when the subtracted values are negative, we replaced the values as zero in the calculation. Then distance estimation and IR reconstruction is performed based on these ISI mitigated samples. The reconstructed IR M_{22} is shown by the light purple curve in (c). Adaptive detection scheme detects the symbol as "1" by comparing reconstructed IR M_{22} and the samples of ISI mitigated signal S_2 in the 2nd interval. The whole process in the 3rd interval is similar to that in the 2nd interval. The only difference is that, instead of only one former symbol in 2nd interval, all the two former symbols are included in the ISI calculation by (4–11). Fig. 4–6 (d) presents the ISI mitigated signals in all the three intervals. Comparing with $C_R(t)$ in (a), the ISI mitigation is effective.

The system model will eventually lose its function as the received moves so far that the estimation of the system parameters and signal detection occurs with a large error. Both the ISI effect and noise contribute to this result. The main reason is that after each ISI mitigation, some ISI molecules still exist and lead to a small error in the distance estimation. The calculated distance for symbol "1" will be further used for ISI mitigation and this error will accumulate and finally disable the system. The noise will also degrade the decoding system.

BER is the direct metric to consider when the system loses its function or become not reliable anymore. When the BER is higher than the pre-set value, we can judge that the system has lose its function. However, BER can't be obtained by the practical demodulator as the true symbol sequence from the transmitter is unknown. Also, it can't expose the effect of a few system parameters on the system's lifetime such as the initial distance, symbol interval, receiver velocity.

Therefore, when the BER has reached the maximum value we set, we adopt the ratio of current symbol "1"'s max concentration to the symbol "1"'s max concentration at initial distance as the metric to judge if the system has reached its lifetime the amplitude. This ratio is decided by the factors of initial distance, symbol interval, receiver velocity and therefore has the potential to describe the system status when it loses its function. We have conducted the experiment to find the metric for the system lifetime. We set the BER standard as the 3e-2 and

Table 4–2 Simulation Parameters

Parameters	Symbol	Values
Symbol sequence	B	7×10^4
Generalized symbol interval	T_m	5
Samples per symbol interval	N_S	5
Signal to noise ratio	SNR	22 dB
Absolute temperature	T	305 K
Diffusion coefficient	D	5 μm^2/s
The number of molecules	N	10^5
Initial distance	d_0	$1.2\,\mathrm{mm}$
Radius of the receiver	a	$1 \times 10^{-4}\,\mathrm{cm}$
Generalized symbol interval	T_m	5
Velocity of the receiver	V_r	2×10^{-3} cm/s
Rotational diffusion coefficient	D_r	5 rad^2/s
Simulation Repeated times		1×10^3

1e-3 for CATD and PAD methods as they fall in the same symbol interval unit, the ultimate ratio is 3.3%. When the mean ratio value in the unit can't satisfy our standard, the system can be considered as "die".

4.2 Simulation Results

In this section, our proposed demodulation scheme is examined by simulations. Important system factors of our proposed schemes are investigated using Monte Carlo simulation. These factors include symbol sequence length B, symbol interval T_b, initial distance d_0, samples per symbol interval N_S and signal to noise ratio (SNR).

4.2.1 Simulation Parameters

In the simulations, flagellated bacterium performing random walk is considered as mobile receiver[42]. We assume that there is no drift velocity in the environment. The released molecules by the transmitter performs Brownian motion[26]. Default parameters adopted are shown in Table 4–2 based on[7, 19]. Different fluid environments and receiver types may have different system parameters. BCSK is adopted as the modulation scheme.

To compare our proposed adaptive demodulation scheme, an adaptive threshold demodulation method is also implemented[25].The threshold can be determined based on MAP detection rule:

$$B_n = \begin{cases} 1, & C_R(t) > \gamma_n, \\ 0, & C_R(t) < \gamma_n. \end{cases} \tag{4–16}$$

where $C_R(t)$ represents the concentration in the n_{th} interval and B_n is the decoded symbol value in the n_{th} interval, γ_n is the threshold in the demodulation system. Note that calculation of γ requires information about the sequence history and we assume the receiver has a memory of ten symbol length memory. The optimal threshold will be obtained through based on the symbol value of the former symbol sequence.

To quantitatively evaluate the performance of the different demodulation schemes, bit error rate (BER) is used as the performance metric in this simulation investigation[30]. All the simulations are conducted in one life time of the system. The complete demodulation algorithm is described in Algorithm 4–1.

4.2.2 Investigation of Symbol Sequence Length

Due to the random walk of the receiver, the increase of released symbol sequence length increases the possibility of a larger distance change with respective to the initial distance d_0. In this subsection, The impact of released symbol sequence length on the performance of demodulation schemes for mobile MC are evaluated. System parameters are set as in Table 4–2.

The simulation result is shown in Fig. 4–7. BER here represents the bit error rate of the entire sequence. All of the three demodulation methods' BER increase as the symbol sequence length increases. Our proposed CATD and PAD demodulation methods outperform the adaptive threshold method.

The adaptive threshold based on the fixed distance considers the former symbols with a static CIR. When the symbol sequence is short (i.e. less than 1×10^4 bits), the distance change is not very obvious and the static CIR can still be used for the calculation of the current CIR. As the symbol sequence increases, the distance change accumulates and current CIR varies significantly than the initial CIR. The adaptive threshold based on the static CIR has a large error than the ideal threshold and the performance degrades gradually.

Meanwhile, BER of both CATD and PAD methods increases as the symbol sequence length increases. The reasons are analyzed as follows. There are two approximations in our proposed scheme. One is the usage of d_{ave} to represent the average dynamic distance range in an interval

算法 **4–1** Adaptive Demodulation Algorithm

Initialization: set $ISIFlag$ = 0, d_{ave} = 0, $formerd$ = initial distance, $decode$ = 0, T_b

for $ii = 1 : B$ **do**

  Sample (t_1, C_1), ...,(t_5, C_5) in current interval;

  Set $C_s = [C_1, C_2, ..., C_5]$;

  if $ISIFlag$!= 0 **then**

    Remove ISI of former bits using based on $formerd$;

  end if

  Calculate current interval's d_{ave} from C_s;

  Reconstruct longTail IR with current d_{ave} using (3–8);

  Record peak point $C_{\max}$ and $T_{\max}$ of this IR;

  Set T_h according to $C_{\max}$;

  Find the max concentration value C_n within interval;

  Decode signal in $decode$ by (4–5) and (4–16) using T_h and C_n;

  if $decode$ == 1 **then**

    $ISIFlag$ = 1;

  end if

  Store distance of latest symbol “1” in $formerd$;

end for=0

and its corresponding IR $C_{\text{ave}}(t)$ to approximate the true IR. The other is the use of the approximated distance d_{ApprDist} and the corresponding IR in the ISI mitigation. Although the parameters are designed to pursue the accuracy of these approximation, differences exist. More importantly, the errors caused by these differences accumulate. For example, there are difference between the IR with approximate distance d_{ApprDist} and the true IR in the ISI mitigation. Therefore in the ISI mitigation, the ISI cannot be removed completely. Residual molecules are left on the samples which are used in the distance estimation and the IR reconstruction for the current interval. There will be errors in the estimated distance and reconstructed IR which further affect the signal detection. Once there is a symbol “1” is decoded incorrectly as “0”, its ISI of this symbol “1” on the following symbols cannot be counted and cannot be removed. This leads to more residual molecules in the following sequence and affects the demodulation in the following intervals. As the released symbol sequence length increases, errors keep accumulating and result in a worse performance with a larger BER.

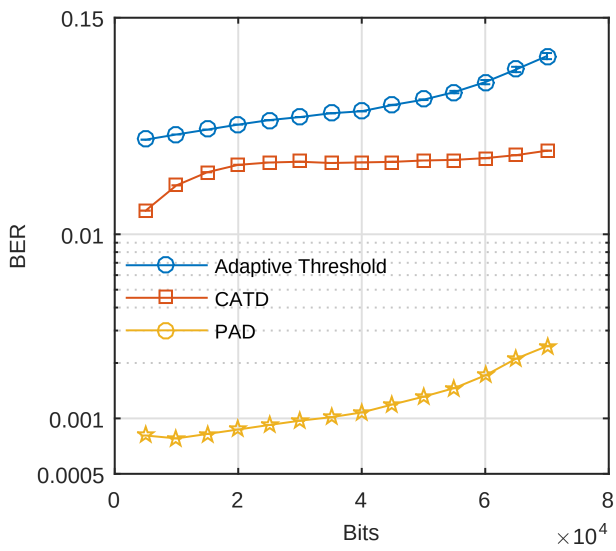

Figure 4–7 The impact of symbol sequence length on the BER performance for different demodulation schemes.

Among the two proposed demodulation methods, PAD performs better than CATD with about one to three orders of magnitude. The reason is that CATD is more sensitive to distance than PAD. Hence, PAD has a better tolerance to the distance error than CATD. In PAD, demodulation is based on the peak time t_{peak}. The peak time value is calculated by (4–6) and its derivative with respect to distance is shown in (4–17) which presents its sensitivity to distance. In CATD, demodulation is based on peak concentration. By substituting t_{peak} of (4–6) into (3–8), peak amplitude C_{peak} for CATD is obtained in (4–18). Its derivative with respect to distance is (4–19) which presents its measurement sensitivity to distance. To compare two methods' sensitivity to distance, we calculate absolute value of (4–17) and (4–19). With parameters in Table 4–2, the absolute value of (4–19) for CATD is larger than that of (4–17) for PAD. This indicates that CATD is more sensitive and easily affected by the distance error than PAD. In the mobile MC, the root error source is the random changes in distance and PAD is more robust to such error than CATD. Hence, PAD performs better than CATD.

$$\frac{\mathrm{d}\, t_{\text{peak}}}{\mathrm{d}\, d_{\text{ave}}} = \frac{d_{\text{ave}}}{3D}, \tag{4–17}$$

$$C_{\text{peak}} = C(t_{\text{peak}}) = \frac{1}{\left(\frac{2\pi}{3}\right)^{\frac{3}{2}} d_{\text{ave}}^{3}} \exp^{-\frac{3}{2}}, \tag{4–18}$$

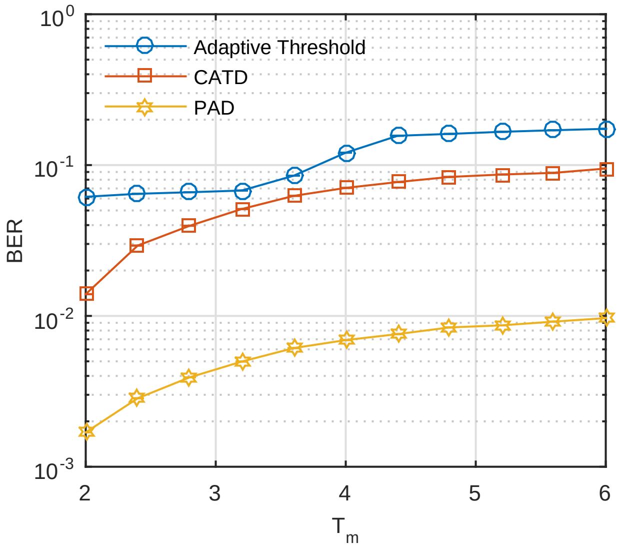

Figure 4–8 The impact of symbol interval on the BER performance of different demodulation schemes for mobile MC.

$$\frac{\mathrm{d}\, C_{\text{peak}}}{\mathrm{d}\, d_{\text{ave}}} = \frac{-3e^{-\frac{3}{2}}}{\left(\frac{2\pi}{3}\right)^{\left(\frac{3}{2}\right)} d_{\text{ave}}^{4}}. \tag{4–19}$$

4.2.3 Investigation of Symbol Interval

Symbol interval is an important parameter in the decoding system. It determines the data rate and affects the ISI effect. Decreasing the symbol interval increases data rate, but aggravates the ISI effect. In this part, the impact of symbol interval on the performance of demodulation schemes of the mobile MC is investigated.

In the simulation, system parameters in Table. 4–2 are adopted. In the environments with different receiver velocity and initial distance, the same T_b has different meaning for ISI mitigation. Therefore normalized T_{norm} in (4–20), instead of T_b, is introduced and investigated in this part. In each run, T_{norm} changes from to 2 to 6 with a step of 0.5.

$$T_{\text{norm}} = \frac{T_b}{T_{\text{peak}}}. \tag{4–20}$$

Simulation result is shown in Fig. 4–8. The proposed CATD and PAD perform better than the adaptive threshold. For the adaptive threshold method, the BER keeps stable before T_m reaches 3. During this period, even the larger interval gives an inaccurate ISI mitigation and a larger error in the distance estimation, the larger interval introduces less ISI molecules into each interval as the CIR falls sharply after peak time. Then the BER increases with respect to T_m. With the increase of T_m, the decrease of ISI is not obvious but the severer distance estimation becomes the main factor in affecting the decoding.

For the proposed CATD and PAD methods, BER increases gradually with respect to T_{norm}. To illustrate such phenomenon, we consider simple case that the increase of T_{norm} is caused by the increase of T_{b} with the same value of T_{peak}. With larger symbol interval T_{b}, dynamic range of the distance in an interval increases and index $k = \frac{V_r \times T_b}{d_0}$ in (4–9) increases too. Therefore d_{ave} is not a good representative of the dynamic range in large interval as in small one. The deviation between the averaged distance d_{ave} and the true distance range in one interval increases. This further causes a larger deviation between the reconstructed IR and true IR. This affects the signal detection accuracy where the reconstructed IR is compared with signal samples to make a decision. Meanwhile, the reconstructed IR is also used in the ISI estimation. Larger deviation reduces the accuracy of the ISI calculation and the effectiveness of the ISI mitigation. Although increasing T_{b} reduces ISI effect, the result manifests that the impact of increased inaccuracy of the reconstructed IR overwhelms the impact of reduced ISI effect and results in larger BER of the proposed demodulation methods.

Among the two proposed methods, PAD performs better than CATD. Similar to the reasons in the investigation of the symbol sequence length, it is because PAD is more robust to distance error in d_{ave}.

4.2.4 Investigation of Initial Distance

System's initial distance d_0 affects index k in (4–9) which determines the relative mobility of the system. The decoding parameters such as the amplitude of the CIR or the peak value time are also affected by the initial distance. In this part, the impact of the initial distance d_0 on the performance of demodulation schemes is investigated. In this simulation, system parameters in Table. 4–2 are adopted. In each run, d_0 changes from to 1 to 5 mm with a step of 0.5 mm.

The simulation result is shown in Fig. 4–9. For adaptive threshold method, its BER increases gradually with initial distance. As the initial distance increases, the amplitude of the CIR is lower and this makes the decoding more easily affected by the noise and ISI.

Both the proposed CATD and PAD method outperform the adaptive threshold method as shown in Fig. 4–9. The BER of both methods decrease as d_0 increases before the initial distance reaches 2.3mm. This is because with larger initial distance d_0, index k in (4–9) decreases.

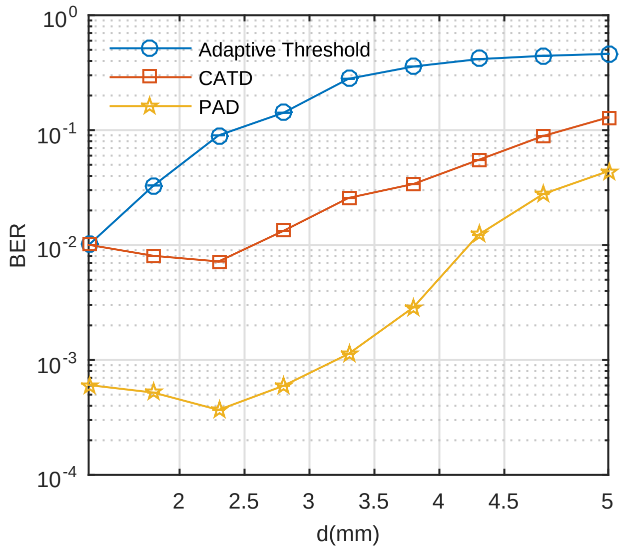

Figure 4–9 The impact of initial distance d_0 on the BER performance of different demodulation schemes for mobile MC.

Smaller k indicates a smaller dynamic range of the distance in an interval. Accordingly, the reconstructed IR with d_{ave} is a better representative of the true IR. The signal detection and ISI mitigation are more effective by using such reconstructed IR. Hence, the demodulation accuracy increases accordingly. However, the BER of both detection methods increases as the initial distance keeps increasing. Amplitude here becomes lower and the decoding process is easily affected by noise and ISI. This reminds us that the initial distance should be controlled when the released molecules number for one symbol is settled.

Among the two proposed methods, PAD outperforms CATD. Similar to the investigations of symbol sequence length and interval, It is because PAD is more robust to distance error.

4.2.5 Investigation of Sampling Number in An Interval

Due to the limitation of energy supply of nanomachines, taking fewer samples in one interval is expected through more samples could provide high accuracy in distance estimation, IR reconstruction and demodulation. Therefore a trade-off arises between the energy saving and accuracy requirement about how many samples to take in an interval. In this part, the impact of sampling numbers N_s in an interval on the performance of demodulation schemes for the mobile MC is investigated. N_s changes from to 1 to 5 with a step of 1.

The result is shown in Fig. 4–10. For adaptive threshold method, as the threshold is de-

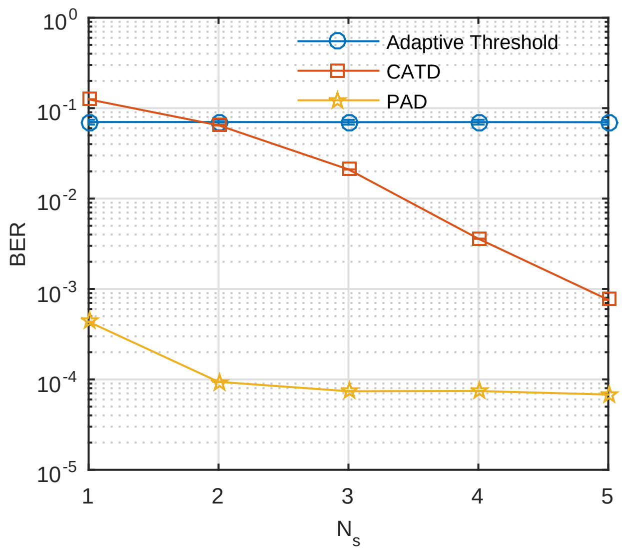

Figure 4–10 The impact of sampling number in an interval on the BER performance of different demodulation schemes for mobile MC.

signed based on the initial CIR, which has been settled, the samples only provide more information for the max concentration. As the first sample has been around the peak location, more samples have only a slight impact on adaptive threshold method. Both of our demodulation methods, CATD and PAD, outperform the adaptive threshold and present a better performance when N_s is larger than 2. For PAD, BER tends to be stable after three sample points cause the sample number has provided enough accuracy for the decoding. As the CATD relies more on the concentration, a larger sample number has a more obvious effect on the decoding.

Among the two proposed methods, PAD outperforms CATD. Similar to the above investigations, it is because that PAD is more robust to distance error and the inaccuracy in the reconstructed IR.

4.2.6 Investigation of Noise

Apart from ISI effect, other noises like the counting noise in MC also has an impact on the decoding process. In the simulation, SNR varies from 16 dB to 26 dB with a step of 2 dB.

Simulation result is shown in Fig. 4–11. The increase of SNR will lead to better performance for all of the three methods. After 18 dB, both our proposed CATD and PAD methods outperform the adaptive threshold demodulation method. With less noise, distance estimation and IR reconstruction are more accurate. ISI mitigation is more effective. Accordingly, the

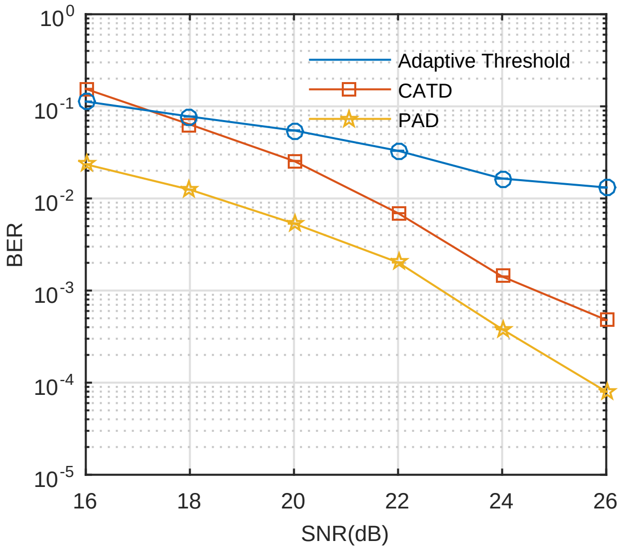

Figure 4–11 The impact of SNR in an interval on the BER performance of different demodulation schemes for the mobile MC.

accuracy of signal detection is improved with a lower BER. Similar to the above investigations, it is because PAD is more robust to distance error and the corresponding inaccuracy in the reconstructed IR.

4.2.7 Summary

In this section, the proposed demodulation schemes CATD and PAD for the mobile MC are examined by simulations.These studies reveal system parameters' impact on the mobile MC. The results show that the adaptive threshold design method used in the static MC fails in the demodulation for the mobile MC. The proposed PAD and CATD perform much better than the adaptive threshold design strategy. Their effectiveness for the mobile MC is demonstrated. Among the two proposed methods, PAD is demonstrated to be more effective and reliable than CATD due to its robustness to distance error.

Chapter 5 High Bit Rate Static MC Scenario

In existing works, much efforts have been taken to fight against ISI. In[9], the authors presented maximum *a posteriori* (MAP) and maximum likelihood (ML) criterions. Then minimum mean square error (MMSE) and a decision-feedback equalizer (DFE) scheme are proposed to mitigate both the ISI and noise in the MC. By utilizing the former symbol sequence and channel sate information, coherent detectors can achieve effective ISI mitigation under low bit rate (i.e. interval time is longer than the peak value time)[9]. However, based on the absolute amplitude of CIR, the detectors are not robust enough to ISI when the data rate gets further higher. As th detectors rely on the information from former sequence, the decoding error will interfere the following decoding process. Some non-coherent detection methods have also been proposed focusing on the characteristics of the channel impulse response (CIR). In[24], the concentration difference in two adjacent intervals is used to decode signal requiring no matrix computation. Using relative amplitude of CIR, this method is less sensitive to heavy ISI while it still needs the information from former symbol. In[45], local convexity is a stable characteristic of the channel response and the detection relying on it requires no information from former symbols. Therefore, it not sensitive to ISI and can be applied into high data rate scenario. Compared with the coherent detectors, non-coherent methods require less former symbol sequence information and are not easily interfered by ISI. However, as the high bit rate scenario can only reveal incomplete and inaccurate CIR characteristic under the heavy effect from ISI and very short symbol interval. The decoding performance based on characteristic like local convexity is limited. To the best of the authors' knowledge, an effective detection technique based on incomplete CIR for the high bit rate scenario in MC is still needed.

In this paper, we propose a non-coherent detector for molecular communication system in high bit rate based on the local derivative of CIR. Displaying the channel impulse response of the MCvD, we observe that the ascending part of the channel response (i.e. the interval before the concentration reaches its maximum value.) is less interfered by ISI in the high bit rate transmission. By employing local fitting technique, we sample the information from the ascending and utilize it to judge the symbol value in the current interval. Pre-smoothing technique is also adopted to mitigate the effect the noise from the environment. As there is no need of information about the former symbol sequence, this method needs less memory resources. Shown in

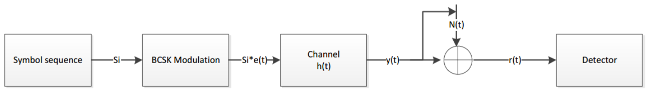

Figure 5–1 Block diagram of the MCvD system

the simulation resources, our proposed scheme is promising in decoding high bit rate signal in MC and robust to the noise and other channel parameters variations.

5.1 System Model

5.1.1 Channel Model

A point-to-point MCvD system is considered in a 3-D unbounded environment. The receiver has a radius of r and a point transmitter is located with a Euclidean distance of d from the receiver. The synchronization of the system is assumed to be accomplished in advance. Binary Concentration Shift Keying (BCSK) is employed as the modulation scheme in this system as in [] and the symbol value is $s_i \in \mathbb{S} = \{0, 1\}, i = 0, 1, \ldots, I$.

A pulse of information molecules is emitted as the transmitter side at the beginning of each time slot T_b. Here we consider the emission pulse to be a rectangular pulse function.

$$E(t) = Xrect(\frac{t - T_e/2}{T_e}) \tag{5–1}$$

where X is the transmission rate[47] and T_e is the emission duration of the transmitter. Generally the emission duration T_e is far shorter than the symbol interval T_b. These molecules diffuse randomly in the environment conforming to Brownian motion. After the propagation process depicted in *Fig.1*, molecules received at the receiver side can be expressed:

$$\begin{aligned} r(t) &= \sum_{i=0}^{\infty} s_i y(t - iT_b) + n_c(t) \\ &= \sum_{i=0}^{\infty} s_i E(t - iT_b) \otimes h(t) + n_c(t) \end{aligned} \tag{5–2}$$

Here $y(t)$ is the noiseless channel response of the signal input and $\otimes$ denotes the convolution operation. s_i is the i_{th} symbol value. Counting noise $n_c(t)$ is introduced by the imperfect counting process happened as the receiver side. $n_{os}(t)$ obeys the normal distribution[46] as:

$n_c(t)$ conforms to the zero-mean white Gaussian distribution[46]:

$$n_c(t) \sim \mathcal{N}(0, \sigma_c^2) \tag{5–3}$$

Distorted by ISI, the received concentration consists of molecules from current symbol and former symbols as well as noise. Meanwhile, as the molecules from previous symbols become negligible after a few bits, the effect from ISI may therefore assumed to come from a finite length e.g. I. The received molecules can be expressed as $\sum_{i=0}^{I} s_i y(t - iT_b)$.

The channel impulse response in our system can be expressed as:

$$h(t) = \frac{1}{(4\pi Dt)^{\frac{3}{2}}} \exp\left(-\frac{|d|^2}{4Dt}\right) \tag{5–4}$$

Here D is the diffusion coefficient decided by both the environment medium and the molecule type.

5.1.2 Bit Rate

In this part, we introduce a generalized definition of bit rate for better evaluation of different MC system. For molecular communication employing BCSK, $1/T_b$ is usually adopted as the bit rate. However, when the diffusion coefficients change in different MC system, shapes of the channel impulse response vary accordingly and the same symbol interval length with T_b actually include CIR information on different scale. Therefore, we consider our transmission rate B_r as:

$$B_r = \frac{T_b}{T_m} \tag{5–5}$$

where T_m is the time location of the peak concentration of the channel response. This can be derived as:

$$T_m = \frac{d^2}{6D} \tag{5–6}$$

5.2 Local Fitting Demodulation Scheme

5.2.1 MAP Coherent Detection in Previous Work

Coherent Detection methods are proposed in the system design of MC due to their appealing performance. MAP framework is commonly adopted in the coherent decoding. In our paper, MAP-based detector is employed to compare with our proposed detector performance. To obtain the decoded symbol sequence $\hat{s}_{0:I}$, MAP detector shall maximize the joint pdf of transmitted symbol sequence $r_{0:I}$ and the received molecule concentration $r_{0:I}$ using Bayes Rule,

$$\begin{aligned}\hat{s}_{0:I} &= \arg\max_{s\in\mathbb{S}} f(r_{0:I}, s_{0:I}) \\ &= \arg\max_{s\in\mathbb{S}} \prod_{i=0}^{I} \Pr(s_i|s_{i+1:I}) \prod_{i=0}^{I} f(r_i|r_{i+1:I}, s_{0:I})\end{aligned} \tag{5–7}$$

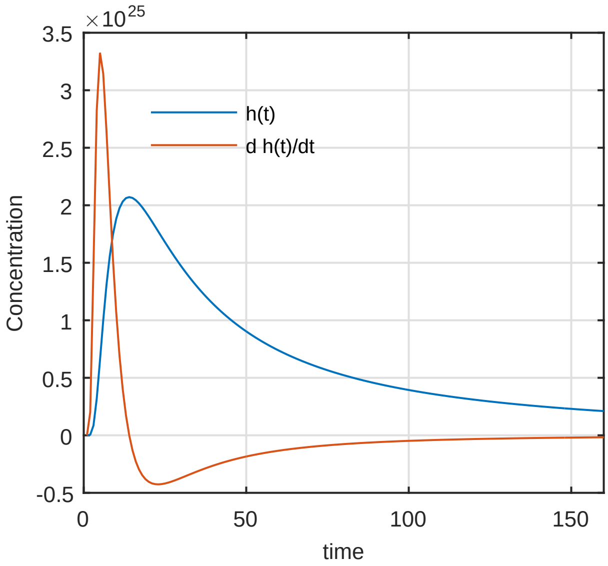

Figure 5–2 Channel impulse response and its derivative.

Here Pr $(s_i|s_{i+1:I})$ is the conditional probability function of the transmitted symbol sequence and $f(r_i|r_{i+1:I}, s_{0:I})$ is conditional pdf following Gaussian distribution[9]. As the transmitted symbol is independent from other ones, Pr $(s_i|s_{i+1:I})$ can be further simplified to Pr (s_i).

5.2.2 Local Fitting Demodulation

Compared with the MC system where $B_r > 1$, high bit rate MC scenarios (e.g. B_r =0.71) bring two disadvantages for decoding process. Heavier ISI is included due to the extremely short symbol interval. Whats' more, we can only obtain part of the CIR information as most of the CIR in cut off by the short T_b. We derive the first order derivative of the channel impulse response $hd(t)$ in (5–8) and observe its plot in Fig. 5–2:

$$hd(t) = \frac{dh(t)}{dt} = \frac{d^2 \exp - \frac{d^2}{4Dt}}{16D^2 \pi t^{\frac{7}{2}}} - \frac{3 \exp - \frac{d^2}{4Dt}}{8D\pi t^{\frac{5}{2}}} \tag{5–8}$$

We can see that there is a sharp peak during the ascending part (i.e. before the max concentration location) of the CIR derivative. By deriving the equation of the CIR's second derivative $\frac{d^2h(t)}{dt^2} = 0$, we can obtain the CIR's peak derivative location:

$$t_{p1} = -\frac{10^{\frac{1}{2}} d^2 - 5d^2}{30D} \quad t_{p2} = \frac{10^{\frac{1}{2}} d^2 + 5d^2}{30D} \tag{5–9}$$

$t_{p1} \approx 0.37T_m$ is the time instance where the derivative has the maximum value and t_{p2} is for the minimum derivative value. Knowing that the maximum derivative is significantly large and its location t_{p1} is in the ascending part of CIR, we then prove that this index can bu used to decode signal even in the presence of severe ISI and it only calls for part of the CIR information.

As stated in section II, we can derive the received signal in the absence of noise:

$$\begin{aligned} r_p(t) &= \sum_{i=0}^{I} s_i y(t - iT_b) \\ &= s_I y(t - IT_b) + \sum_{i=0}^{I-1} s_i y(t - iT_b) \end{aligned} \tag{5–10}$$

As the emission time is sufficiently smaller than the symbol interval, $e(t) \otimes h(t)$ can be approximated as $Xh(t)$ and the derivative of $r(t)$ can be expressed as:

$$r_p(t) = s_I X h(t - IT_b) + \sum_{i=0}^{I-1} s_i X h(t - iT_b) \tag{5–11}$$

$$\frac{\partial r(t)}{\partial t} = \sum_{i=0}^{I} hd(t_{p1} + iT_b) \tag{5–12}$$

As t_{p1}, T_m and T_b can all be expressed in terms of parameters D and d, $hd(t_{p1} + iT_b)$ can be expressed as the function $hd(D, d)$. Then we consider an extremely high bit rate scenario where $T_b \approx 0.71T_m$. In the previous work, the finite ISI length is usually less than two bits and we firstly adopt a four bits symbol-one length ISI sequence due to the severer ISI effect of a shorter symbol interval. With a positive constant parameter D, $hd(D, d)$ is a monotonic function and we have:

$$\lim_{d \to \infty} hd(D, d) = 0 \quad D \in \mathbb{R}^+ \tag{5–13}$$

We can find that the sum of the derivative is always beyond zero when the current symbol value is one. Then we expand the ISI sequence to five bits interference, by calculating its stationary point and hessian matrix. We found the fifth symbol's derivative influence can be neglected showing that considering four-bit length ISI is enough for our demodulation method.

As the derivative from previous symbols are all negative, its easy to observe that the derivative is negative when the current symbol value is zero. Therefore, we can obtain an approximating derivative around t_{p1} to decode current symbol:

$$d_r \gtrless_0^1 \delta \tag{5–14}$$

where d_r is the index we calculate from the actual concentration by local fitting and δ is the local fitting index from symbol one. This is especially suitable for the high bit scenario as we don't need the information from the descending out of the interval bound. Note that this metric can be slightly adjusted considering the effect from the noise. Discussions are conducted in the simulation part.

5.2.3 Noise Mitigation and Derivative Calculation

Noise-mitigating has to be conducted before we use the signal for the next step processing. For our MC system, in the equivalent discrete signal model we have

$$r(m) = s_0 h(m) + \sum_{i=0}^{I} s_i h(m - iT_b) \tag{5–15}$$

$$h(m) = \sum_{n=-N}^{N} h(m - t_{p1} - nT_s) \tag{5–16}$$

where T_s is the oversampling rate set as $1/t_m$. Now we have a sample sequence with a length of 2N+1 in each interval: $c = [c_1, \ldots, c_{2N+1}]$. We then conduct the ISI mitigating process between $(K+1)_{th}$ and $(2N-K)_{th}$ sample:

$$c_i' = \frac{\sum_{l=i-K}^{i+K} c_l}{2K+1} \tag{5–17}$$

After mitigating the noise effect, we use local fitting method to get the first order fitting index of the samples. The local derivative we desire can be solved Using Vandermonde determinant.

5.3 Simulation Results

In this section, our local fitting detection method is examined through Monte Carlo simulation. The trade off between the bit rate and system performance is evaluated firstly and then we forward to discuss the proper range in the metric design. 1×10^5 symbols are transmitted randomly in each simulation. Bit Error Rate (BER) is employed to evaluate our system performance. As noise is considered in our system, we define the signal to noise ratio (SNR) in logarithmic decibel scale as:

$$SNR \triangleq 10\log_{10}(\frac{P_r}{P_N}) \triangleq 10\log_{10}(\frac{\frac{1}{I+1}\sum_{i=0}^{I} r_i^2}{\mathbb{E}[\delta_N^2]}) \tag{5–18}$$

where P_r and P_N is the signal power and the noise power, δ_N^2 is the variance of the combined noise. r_i is the average signal amplitude in an interval.

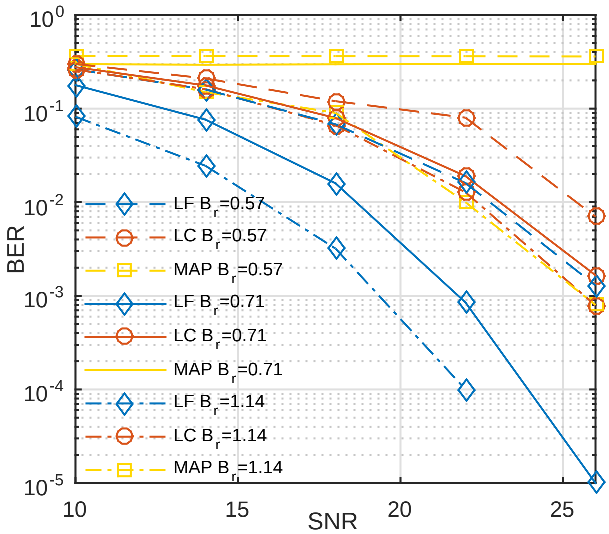

Figure 5–3 BER performance for MAP, local convexity and LF detector. Three time interval is discusses to investigate the detector performance in different bit rate scenarios.

Channel Parameters have to be set in advance and we assume that the receiver side has already known the time location of t_{p1} in one interval. This can be achieved by sending a sequence of pilot symbols. In our high data rate scenarios, symbol interval can be set shorter than the peak value time T_m but need to be longer than t_{p1}. We arrange $D = 4.8 \times 10^{-8} m^2/s$ and $d = 65nm$[45]. MAP coherent detector[9] and local convexity non-coherent[45] are compared with our LF non-coherent detector.

In the first experiment shown in Fig. 5–2, we investigate the performance difference when the factors B_r and SNR varies. Shown in Fig. 5–3, both of the two non-coherent detectors behave better under the low influence of noise. However, the MAP method ($I = 15$) has a poor performance when the data rate is extremely high (e.g. $B_r = 0.57\&0.71$), this is because the incomplete CIR information (i.e. receiver can only obtain samples from ascending part constrained by the short interval.) and severe ISI can't enable MAP detector to make an accurate detection and estimation. The MAP detector is not reliable anymore in this scenario. Our LF detector has excellent BER performance in high bit rate and it is also suitable for the scenario where T_b is larger than T_m. This result indicates our detector is robust in the high bit rate and also has a wide range of application scenarios.

In the next experiment, we focus on the metric design of the detector in high bit rate ($B_r = 0.71$). Considering the energy consumption, we only sample five points around t_{p1} universally

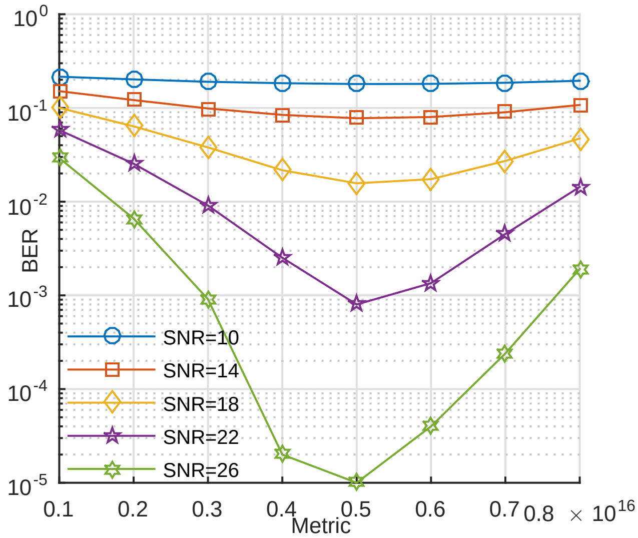

Figure 5–4 Channel impulse response and its derivative

with a interval of $T_s = 1.06 \times 10^{-9}$. In the ideal situation without noise, we calculate the local derivate around t_{p1} and set half of its value as metric δ. In our case, the ideal metric is $\delta = 0.7 \times 10^{16}$. However, we find that the system has the best performance around 0.5×10^{16}. This is because true ISI comes from a infinite sequence and the actual derivative is lower than the analytical one. What's more, the noise effect may slightly distract the LF calculation and therefore some calculation results from symbol ones may also have a lower value than the ideal one.

Chapter 6 Conclusion

In this paper, we propose a demodulation scheme for the mobile MC. For the mobile MC scenario, a well studied flagellated bacteria, E.coli, is considered as a mobile receiver performing random walk. Three-dimensional channel model is established considering the random walk of E. coli as the mobile receiver. For the mobile MC, current demodulation schemes do not work due to the randomness of the IR of the mobile channel. In this paper, adaptive demodulation scheme is proposed for the mobile MC. This adaptive demodulation scheme includes three main parts which are adaptive ISI mitigation, distance estimation and IR reconstruction, and two adaptive detection methods PAD and CATD. These three parts are proposed specifically for the mobile MC.

The proposed demodulation scheme is verified by Monte Carlo simulations. The simulation results show that the proposed demodulation scheme performs better than the adaptive threshold strategy for the static MC. Among the two detection schemes, PAD outperforms CATD. Therefore, we recommend PAD for demodulation in the mobile MC. The impacts of important system factors including symbol sequence length, symbol interval, initial distance, sampling number in one interval and SNR, are also studied. These studies reveal the rules of the impacts of these factors which could be used to optimize the system performance.

In future, there are open issues to be solved. Firstly, the data rate in the current system is too low. High data rate scenario detection remains to be solved for our demodulation schemes. Also, demodulation schemes for other modulation methods such as MoSK in the mobile MC should also be investigated and compared.

[Proof of the System Error Probability]

For the channel impulse response of our system in (3–9), we consider it as the probability density function of the sensed concentration at time t. Therefore, it can be represented as $P_{ob}(D, d, t)$ in terms of parameters of Diffusion coefficient, distance d and time t.For the current symbol, the received concentration includes the transmitted molecules from current symbol and residual molecules as ISI. Also, the counting noise should also be included in our analytical expression. We have the received concentration as:

$$C_R(t) = C_0(t)S_0 + \sum_{i=1}^{I} C_i(t)S_i + n_{cs} \tag{–1}$$

$C_i(t)$ here can be expressed as $C_0(t + iT_b)$. N_{cs} represents the value of the counting noise. S_i represents the symbol value of the i_{th} symbol. $C_0(t)S_0$ is the concentration from the current symbol and it obeys the binomial distribution:

$$C_0(t)S_0 \sim \mathcal{B}(NS_0, P_0) \tag{–2}$$

P_0 can be expressed as $P_{ob}(D, d_c, t)$ and d_c is the distance for current time t. For the ISI effect with a symbol length of I, the concentration from each symbol also complies to the binomial distribution:

$$C_i(t)S_i \sim \mathcal{B}(NS_i, P_i - P_{i-1}) \tag{–3}$$

After sampling the current concentration, we need to mitigate the ISI for the further demodulation. We reconstructed the CIR for the former symbols using our storage distance df and the mitigated signal CRM become:

$$C_R(t) = C_0(t)S_0 + \sum_{i=1}^{I} C_i(t)S_i - \sum_{i=1}^{I} C_{ir}(t)S_{ir} + N_{cs} \tag{–4}$$

Where $C_{ir}(t)$ and S_{ir} are the estimated concentration and symbol values and the estimated concentration also complies to the binomial distribution:

$$C_{ir}(t)S_{ir} \sim \mathcal{B}(NS_{ir}, P_{ir} - P_{ir-1}) \tag{–5}$$

The difference from the actual ISI signal is that P_{ir} represents $P_{ob}(D, d_e, t + iTb)$ and d_e represents the distance for the last symbol one. As the transmitted molecules N are large enough, the binomial distribution can be approximated to the normal distribution and our mitigated signal can be expressed as:

$$\begin{aligned} C_{RM}(t) \sim \mathcal{N}&(NS_0P_0, NS_0P_0(1-P_0)) \\ &+ N(NS_iQ_i, NS_iQ_i(1-Q_i)) \\ &- N(NS_{ir}Q_{ir}, NS_{ir}Q_{ir}(1-Q_{ir})) + N(0, \sigma_{cs}^2) \end{aligned} \tag{–6}$$

Here $Q_i = P_i – P_i - 1$ and $Q_{ir} = P_{ir} – P_{ir} - 1$. Referring[64], we can derive the error probability for the CATD detection method:

$$\begin{aligned} P_e &= M_0 \,\mathbf{Pr}(S_r = 1|S_0 = 0) + M_1 \,\mathbf{Pr}(S_r = 0|S_0 = 1) \\ &= \frac{M_1}{2}(1 + erf(\frac{\tau - \mu_1}{\sqrt{2\sigma_1{}^2}})) + \frac{M_0}{2}(1 - erf(\frac{\tau - \mu_0}{\sqrt{2\sigma_0{}^2}})) \end{aligned} \tag{–7}$$

Here we assume the probability of sending symbol one in the current symbol is M_1 and the probability for symbol zero is M_0. For PAD detection method, we need to calculate the peak value time from the distance we derived and utilizes this index to decode. However, as the distance between the transmitter and the receiver is hard to predict and we haven’t reached an analytical expression for the distance between the transmitter and the receiver under the mobile situation. The error probability is still hard to estimate or exposed in the numerical results.

References

[1] AKYILDIZ I F, JORNET J M, PIEROBON M. Nanonetworks: A new frontier in communications[J]. Commun. ACM, 2011, 54(11): 84–89.

[2] NAKANO T, MOORE M J, WEI F, et al. Molecular communication and networking: Opportunities and challenges[J]. IEEE Trans. Nanobiosci., 2012, 11(2): 135–148.

[3] NAKANO T, SUDA T, OKAIE Y, et al. Molecular communication among biological nanomachines: A layered architecture and research issues[J]. IEEE Trans. Nanobiosci., 2014, 13(3): 169–197.

[4] BACA H K, CARNES E C, ASHLEY C E, et al. Cell-directed-assembly: directing the formation of nano/bio interfaces and architectures with living cells[J]. Biochimica et Biophysica Acta (BBA)-General Subjects, 2011, 1810(3): 259–267.

[5] GUPTA R, SHARMA M, MITTAL A. Effects of membrane tension on nanopropeller driven bacterial motion[J]. Journal of Nanoscience and Nanotechnology, 2006, 6(12): 3854–3862.

[6] LENTINI R, SANTERO S P, CHIZZOLINI F, et al. Integrating artificial with natural cells to translate chemical messages that direct E. coli behaviour[J]. Nature Communications, 2014, 5.

[7] OKAIE Y, NAKANO T, HARA T, et al. Cooperative Target Tracking by a Mobile Bionanosensor Network[J]. English. IEEE Trans. Nanobiosci., 2014, 13(3): 267–277. DOI: {10.1109/TNB.2014.2343237}. ISSN: 1536-1241.

[8] MENG L.-S, YEH P.-C, CHEN K.-C, et al. On receiver design for diffusion-based molecular communication[J]. IEEE Trans. Signal Process., 2014, 62(22): 6032–6044.

[9] KILINC D, AKAN O B. Receiver design for molecular communication[J]. IEEE J. Sel. Areas Commun., 2013, 31(12): 705–714.

[10] FARSAD N, YILMAZ H B, ECKFORD A, et al. A Comprehensive Survey of Recent Advancements in Molecular Communication[J]. IEEE Commun. Surveys Tuts, 2016, 18(3): 1887–1919. DOI: 10.1109/COMST.2016.2527741. ISSN: 1553-877X.

[11] KIM N.-R, CHAE C.-B. Novel modulation techniques using isomers as messenger molecules for nano communication networks via diffusion[J]. IEEE J. Sel. Areas Commun., 2013, 31(12): 847–856.

[12] PIEROBON M, AKYILDIZ I F. Diffusion-based noise analysis for molecular communication in nanonetworks[J]. IEEE Trans. Signal Process., 2011, 59(6): 2532–2547.

[13] GUNEY A, ATAKAN B, AKAN O B. Mobile ad hoc nanonetworks with collision-based molecular communication[J]. IEEE Trans. Mobile Comput., 2012, 11(3): 353–366.

[14] FELICETTI L, FEMMINELLA M, REALI G. Establishing digital molecular communications in blood vessels[C]// Proc. IEEE BlackSeaCom. [S.l.]: [s.n.], 2013: 54–58.

[15] LUO Z, LIN L, MA M. Offset estimation for clock synchronization in mobile molecular communication system[C]// Proc. IEEE WCNC. IEEE. [S.l.]: [s.n.], 2016: 1–6.

[16] KUSCU M, AKAN O B. A communication theoretical analysis of FRET-based mobile ad hoc molecular nanonetworks[J]. IEEE Trans. Nanobiosci., 2014, 13(3): 255–266.

[17] KUSCU M, AKAN O B. Coverage and throughput analysis for FRET-based mobile molecular sensor/actor nanonetworks[J]. Nano Commun. Netw., 2014, 5(1): 45–53.

[18] QIU S, ASYHARI T, GUO W. Mobile molecular communications: Positional-distance codes[C]// Proc. IEEE 17th International Workshop on Signal Processing Advances in Wireless Communications (SPAWC). [S.l.]: [s.n.], 2016: 1–5. DOI: 10.1109/SPAWC.2016.7536830.

[19] BERG H C. Random walks in biology[M]. [S.l.]: Princeton University Press, 1993.

[20] AHMADZADEH A, JAMALI V, NOEL A, et al. Diffusive Mobile Molecular Communications Over Time-Variant Channels[J]. IEEE Communications Letters, 2017.

[21] WANG Z, KIM M, ROSEN G. Validating models of bacterial chemotaxis by simulating the random motility coefficient[J]. 2008: 1–5.

[22] MAHFUZ M U, MAKRAKIS D, MOUFTAH H T. On the characterization of binary concentration-encoded molecular communication in nanonetworks[J]. Nano Commun. Netw., 2010, 1(4): 289–300.

[23] LLATSER I, ALARCÓN E, PIEROBONY M. Diffusion-based channel characterization in molecular nanonetworks[C]// Proc. IEEE INFOCOM. IEEE. [S.l.]: [s.n.], 2011: 467–472.

[24] LI B, SUN M, WANG S, et al. Low-complexity noncoherent signal detection for nanoscale molecular communications[J]. IEEE Trans. Nanobiosci., 2016, 15(1): 3–10.

[25] TEPEKULE B, PUSANE A E, YILMAZ H B, et al. ISI mitigation techniques in molecular communication[J]. IEEE Trans. Mol. Biol. Multi-Scale Commun., 2015, 1(2): 202–216.

[26] GUO W, ASYHARI T, FARSAD N, et al. Molecular communications: channel model and physical layer techniques[J]. IEEE Wireless Communications, 2016, 23(4): 120–127. DOI: 10.1109/MWC.2016.7553035. ISSN: 1536-1284.

[27] KURAN M S, YILMAZ H B, TUGCU T, et al. Modulation techniques for communication via diffusion in nanonetworks[C]// Proc. IEEE ICC. IEEE. [S.l.]: [s.n.], 2011: 1–5.

[28] MAHFUZ M U, MAKRAKIS D, MOUFTAH H T. A generalized strength-based signal detection model for concentration-encoded molecular communication[C]// Proc. The 8th International Conference on Body Area Networks. ICST (Institute for Computer Sciences, Social-Informatics, Telecommunications Engineering). [S.l.]: [s.n.], 2013: 461–467.

[29] LIN W.-A, LEE Y.-C, YEH P.-C, et al. Signal detection and ISI cancellation for quantity-based amplitude modulation in diffusion-based molecular communications[C]// Proc. IEEE GLOBECOM. IEEE. [S.l.]: [s.n.], 2012: 4362–4367.

[30] AIJAZ A, AGHVAMI A.-H. Error performance of diffusion-based molecular communication using pulse-based modulation[J]. IEEE Trans. Nanobiosci., 2015, 14(1): 146–151.

[31] MAHFUZ M U, MAKRAKIS D, MOUFTAH H T. A comprehensive analysis of strength-based optimum signal detection in concentration-encoded molecular communication with spike transmission[J]. IEEE Trans. Nanobiosci., 2015, 14(1): 67–83.

[32] CHOU C T. A Markovian approach to the optimal demodulation of diffusion-based molecular communication networks[J]. IEEE Trans. Commun., 2015, 63(10): 3728–3743.

[33] SHAHMOHAMMADIAN H, MESSIER G G, MAGIEROWSKI S. Optimum receiver for molecule shift keying modulation in diffusion-based molecular communication channels[J]. Nano Commun. Netw., 2012, 3(3): 183–195.

[34] LIN Y.-K, LIN W.-A, LEE C.-H, et al. Asynchronous Threshold-Based Detection for Quantity-Type-Modulated Molecular Communication Systems[J]. IEEE Trans. Mol. Biol. Multi-Scale Commun., 2015, 1(1): 37–49.

[35] NOEL A, CHEUNG K C, SCHOBER R. Optimal receiver design for diffusive molecular communication with flow and additive noise[J]. IEEE Trans. Nanobiosci., 2014, 13(3): 350–362.

[36] KOO B H, YILMAZ H B, CHAE C.-B, et al. Detection algorithms for molecular MIMO[C]// Proc. IEEE ICC. IEEE. [S.l.]: [s.n.], 2015: 1122–1127.

[37] MOORE M J, NAKANO T, ENOMOTO A, et al. Measuring distance from single spike feedback signals in molecular communication[J]. IEEE Transactions on Signal Processing, 2012, 60(7): 3576–3587.

[38] NOEL A, CHEUNG K C, SCHOBER R. Bounds on distance estimation via diffusive molecular communication[C]// Global Communications Conference (GLOBECOM), 2014 IEEE. IEEE. [S.l.]: [s.n.], 2014: 2813–2819.

[39] NOEL A, CHEUNG K C, SCHOBER R. Joint channel parameter estimation via diffusive molecular communication[J]. IEEE Trans. Mol. Biol. Multi-Scale Commun., 2015, 1(1): 4–17.

[40] WANG X, HIGGINS M D, LEESON M S. Distance estimation schemes for diffusion based molecular communication systems[J]. IEEE Communications Letters, 2015, 19(3): 399–402.

[41] AKYILDIZ I F, BRUNETTI F, BLÁZQUEZ C. Nanonetworks: A new communication paradigm[J]. Computer Netw., 2008, 52(12): 2260–2279.

[42] GREGORI M, AKYILDIZ I F. A new nanonetwork architecture using flagellated bacteria and catalytic nanomotors[J]. IEEE J. Sel. Areas Commun., 2010, 28(4): 612–619.

[43] TINDALL M J, PORTER S, MAINI P, et al. Overview of mathematical approaches used to model bacterial chemotaxis I: the single cell[J]. Bulletin of mathematical biology, 2008, 70(6): 1525–1569.

[44] NOEL A, CHEUNG K C, SCHOBER R. A unifying model for external noise sources and ISI in diffusive molecular communication[J]. IEEE Journal on Selected Areas in Communications, 2014, 32(12): 2330–2343.

[45] LI B, SUN M, WANG S, et al. Local Convexity Inspired Low-Complexity Noncoherent Signal Detector for Nanoscale Molecular Communications[J]. IEEE Trans. Commun., 2016, 64(5): 2079–2091.

[46] SINGHAL A, MALLIK R K, LALL B. Performance analysis of amplitude modulation schemes for diffusion-based molecular communication[J]. IEEE Transactions on Wireless Communications, 2015, 14(10): 5681–5691.

[47] MOSAYEBI R, ARJMANDI H, GOHARI A, et al. Receivers for diffusion-based molecular communication: Exploiting memory and sampling rate[J]. IEEE Journal on Selected Areas in Communications, 2014, 32(12): 2368–2380.

[48] MENG L.-S, YEH P.-C, CHEN K.-C, et al. Optimal detection for diffusion-based communications in the presence of ISI[C]// Proc. IEEE GLOBECOM. IEEE. [S.l.]: [s.n.], 2012: 3819–3824.

[49] AHMADZADEH A, NOEL A, SCHOBER R. Analysis and design of multi-hop diffusion-based molecular communication networks[J]. IEEE Trans. Mol. Biol. Multi-Scale Commun., 2015, 1(2): 144–157.

[50] AKKAYA A, YILMAZ H B, CHAE C.-B, et al. Effect of receptor density and size on signal reception in molecular communication via diffusion with an absorbing receiver[J]. IEEE Commun. Lett., 2015, 19(2): 155–158.

[51] GUO W, LI B, WANG S, et al. Molecular communications with longitudinal carrier waves: baseband to passband modulation[J]. IEEE Commun. Lett., 2015, 19(9): 1512–1515.

[52] KIM N.-R, ECKFORD A W, CHAE C.-B. Symbol Interval Optimization for Molecular Communication With Drift[J]. IEEE Trans. Nanobiosci., 2014, 13(3): 223–229. DOI: {10.1109/TNB.2014.2342259}. ISSN: 1536-1241.

[53] MOVAHEDNASAB M, SOLEIMANIFAR M, GOHARI A, et al. Adaptive transmission rate with a fixed threshold decoder for diffusion-based molecular communication[J]. IEEE Trans. Commun., 2016, 64(1): 236–248.

[54] NAKANO T, ECKFORD A W, HARAGUCHI T. Molecular communication[M]. [S.l.]: Cambridge University Press, 2013.

[55] NOEL A, CHEUNG K C, SCHOBER R. Improving receiver performance of diffusive molecular communication with enzymes[J]. IEEE Trans. Nanobiosci., 2014, 13(1): 31–43.

[56] OKAIE Y, NAKANO T, HARA T, et al. Modeling and performance evaluation of mobile bionanosensor networks for target tracking[J]. 2014: 3969–3974.

[57] OKAIE Y, NAKANO T, HARA T, et al. Cooperative target tracking by a mobile bionanosensor network[J]. IEEE Trans. Nanobiosci., 2014, 13(3): 267–277.

[58] SHAHMOHAMMADIAN H, MESSIER G G, MAGIEROWSKI S. Blind synchronization in diffusion-based molecular communication channels[J]. IEEE Commun. Lett., 2013, 17(11): 2156–2159.

[59] YILMAZ H B, CHAE C.-B. Simulation study of molecular communication systems with an absorbing receiver: Modulation and ISI mitigation techniques[J]. Simulation Modelling Practice and Theory, 2014, 49: 136–150.

[60] SAFFMAN M P G; Delbruck. Brownian motion in biological membranes[J]. Proceedings of the National Academy of Sciences of the United States of America, 1975, 72(8): 3111–3113.

[61] AKYILDIZ I F, BRUNETTI F, BLÁZQUEZ C. Nanonetworks: A new communication paradigm[J]. Computer Networks, 2008, 52(12): 2260–2279.

[62] LUO Z, LIN L, MA M. Offset estimation for clock synchronization in mobile molecular communication system[C]// Wireless Communications and Networking Conference (WCNC), 2016 IEEE. IEEE. [S.l.]: [s.n.], 2016: 1–6.

[63] LI B, SUN M, WANG S, et al. Local convexity inspired low-complexity noncoherent signal detector for nanoscale molecular communications[J]. IEEE Transactions on Communications, 2016, 64(5): 2079–2091.

[64] TAVAKKOLI N, AZMI P, MOKARI N. Performance Evaluation and Optimal Detection of Relay-Assisted Diffusion-Based Molecular Communication With Drift[J]. IEEE transactions on nanobioscience, 2017, 16(1): 34–42.

[65] KILINC D, AKAN O B. Receiver design for molecular communication[J]. IEEE Journal on Selected Areas in Communications, 2013, 31(12): 705–714.

[66] MOORE M J, NAKANO T, ENOMOTO A, et al. Measuring distance from single spike feedback signals in molecular communication[J]. IEEE Transactions on Signal Processing, 2012, 60(7): 3576–3587.

[67] NOEL A, CHEUNG K C, SCHOBER R. Bounds on distance estimation via diffusive molecular communication[C]//Global Communications Conference (GLOBECOM), 2014 IEEE. IEEE. [S.l.]: [s.n.], 2014: 2813–2819.

[68] FARSAD N, YILMAZ H B, ECKFORD A, et al. A comprehensive survey of recent advancements in molecular communication[J]. IEEE Communications Surveys & Tutorials, 2016, 18(3): 1887–1919.

[69] LI B, SUN M, WANG S, et al. Low-complexity noncoherent signal detection for nanoscale molecular communications[J]. IEEE transactions on nanobioscience, 2016, 15(1): 3–10.

[70] MOORE M J, SUDA T, OIWA K. Molecular communication: Modeling noise effects on information rate[J]. IEEE transactions on nanobioscience, 2009, 8(2): 169–180.

[71] SINGHAL A, MALLIK R K, LALL B. Performance analysis of amplitude modulation schemes for diffusion-based molecular communication[J]. IEEE Transactions on Wireless Communications, 2015, 14(10): 5681–5691.

[72] KILINC D, AKAN O B. Receiver design for molecular communication[J]. IEEE Journal on Selected Areas in Communications, 2013, 31(12): 705–714.

[73] LI B, SUN M, WANG S, et al. Local convexity inspired low-complexity noncoherent signal detector for nanoscale molecular communications[J]. IEEE Transactions on Communications, 2016, 64(5): 2079–2091.

Published Papers during Undergraduate Study

[1] **Ge Chang**, Hao Yan, "*Local Fitting Signal Detection for Molecular Communication for High Bit Rate System,*" in IEEE COMMUNICATION LETTER. (**To be submitted**)

[2] **Ge Chang**, Hao Yan "*Adaptive Demodulation For Mobile Receivers With ISI Mitigation In Molecular Communication,*" in IEEE TRANSACTIONS ON NANOBIOSCIENCE.(**In Major Revision**)

[3] Hao Yan, **Ge Chang**, Haotian Sun, Xuying Zhan, Zhongke Ma, Zhou Tao, Lin Lin, "*Molecular Communication in Nanonetworks,*" in Nano Biomed. Eng, 2016, 8(4): 274-287G. (**Supervisor First Author**)

[4] Haotian Gao, Senlin Zhu, **Ge Chang**, Lingfeng Fu, Zhenyu Huang, "*Architecture and Realization of Intelligent Greenhouse System Based on Agricultural Internet of Things,*" in CHINESE JOURNAL OF AGRICULTURAL MACHINERY.(**Published**)

Acknowledgements

首先我要感谢我的导师闫浩老师, 在我的本科阶段以及整个毕业设计过程中对我各方面的悉心指导。进入了闫老师分子通信研究组后，我们进行了各个方向的有深度与广度的学习。在毕业设计的选题上，闫老师对我们进行积极的引导，并且给予了我很大的选择自由，让我能够自由地选择自己的题目。在整个项目开展期间，闫老师和我进行了多次研究与讨论并且将自己的研究成果与技术耐心的教导与我，让我能够快速找到应对方式与方法解决所遇到的问题。第一次撰写论文遇到了无数问题, 闫老师总会及时的给予我鼓励与帮助, 传授给我撰写论文的经验与技巧。闫老师的耐心指导与帮助是我圆满完成毕业设计的关键。

同时我也要感谢林林老师对我的帮助，在修改论文期间，林林老师不辞辛苦，投入大量的时间与我一起探讨问题，在这期间我们不断产生新的思路，对拓展研究深度和广度有着极为重要的意义。

同时我还要感谢毛义梅老师，茅旭初老师在毕业设计的相关问题上给予我的细心解答和帮助，让我能够在规定节点内更好的完成我的研究内容。

同时, 感谢分子通信组的同学们。我在实验室的这一年里，他们给了我很多直接或间接的帮助。我在这里学到了很多关于研究的知识和方法。我由衷的庆幸我能够和这样一群人共同学习研究。

还要感谢我的朋友和同学们。他们在这四年里帮助了我很多，在我沮丧无助的时候向我伸出援手。他们中的一些也对我的研究参与了讨论，提出看很多值得参考的意见。

最后，我要感谢我深爱的家人。他们关心着我生活的各个方面，同时也在物质上支持着我的学业。正因为他们的一路支持我才能走到这里。